Journal of Sound and Vibration (2002) **258**(1), 65–94
doi:10.1006/jsvi.5089, available online at http://www.idealibrary.com on IDEAL®

DYNAMIC STABILITY OF TRAINS MOVING OVER BRIDGES SHAKEN BY EARTHQUAKES

Y.-B. YANG AND Y.-S. WU

Department of Civil Engineering, National Taiwan University, Taipei 10617, *Taiwan, Republic of China.*
E-mail: ybyang@ccms.ntu.edu.tw

(*Received* 31 *July* 2001, *and in final form* 27 *February* 2002)

The dynamic stability of trains moving over bridges shaken by earthquakes is studied. Unlike the seismic analysis of structures containing a single subsystem, the seismic analysis of a bridge sustaining a passing train requires not only information on acceleration, but also on velocity and displacement of the ground motion. Four typical earthquakes, including the 1999 Chi-Chi Earthquake, were adopted as the input excitations, each of which was normalized to have a moderate intensity. The results indicate that a train initially resting on the bridge can stay safely under the ground motions considered, if the bridge and track structures do not exhibit inelastic deformations during the earthquake. The type of the vertical component of ground motions can affect significantly the stability of the train–rail–bridge system. As a preliminary attempt, safety, possible instability and instability regions were established in a three-phase plot for the train running over the bridge for each of the earthquakes considered, from which the maximum allowable speed for the train to run safely under the specified ground acceleration can be obtained.

1. INTRODUCTION

Seismic resistance of bridge structures is an issue of great concern in many countries, especially those located in earthquake-prone regions. As for railway bridges, it is possible that the bridge itself may remain safe during an earthquake, but may not be safe enough for the trains to move over it due to excessive vibrations. Evidently, the safety of moving trains over the bridge under earthquake excitations is a subject of great concern in railway engineering. This problem is becoming more important because of the frequent use of elevated bridges as railway supporting structures nowadays and because of the increase in running speed of passenger trains. To the knowledge of the authors, however, rather limited efforts have been devoted to this problem in the past. In the study by Miura [1], emphasis was placed on the earthquake-induced displacement of tracks and structures as well as the damage of trains to earthquake excitations, rather than on the dynamic stability of trains under earthquakes. Miyamoto *et al.* [2] investigated analytically the running safety of railway vehicles under the action of earthquakes using a three-dimensional (3-D) simplified vehicle model, where sine waves are used as the input excitation and the vehicle is set to be stationary on the track. Ma and Zhu [3] studied the response of high-speed trains and continuous rigid-frame bridges under three different ground motions by the random vibration theory. In their work, the track system was not taken into account, while only ground motions with two specific intensities were considered, which may not be satisfactory in practice, as the trains may be attacked by earthquakes of various intensities.

0022-460X/02/$35.00

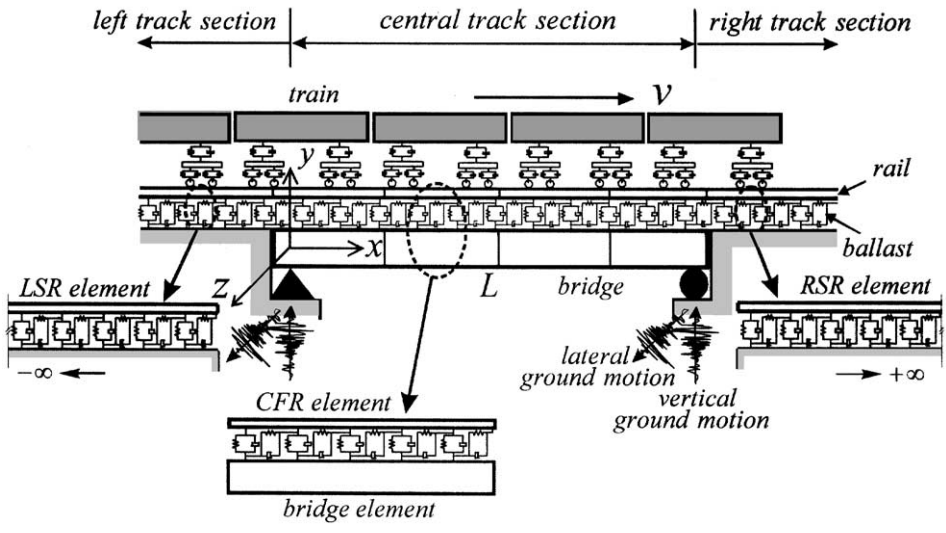

Figure 1. A train travelling over a simply supported railway bridge shaken by earthquakes.

In this paper, the stability of trains initially resting on or travelling over bridges under different seismic excitations will be investigated using 3-D train and bridge models, with the effect of the track system taken into account. As a preliminary effort toward assessment of the safety of moving trains shaken by earthquakes, the bridge is assumed to remain elastic during the earthquake, while some simple criteria, such as the derailment index, are adopted for evaluating the safety of the moving train. It is realized that margin does exist for improving the train and bridge models, for instance, the bridge may display inelastic behaviour during the earthquake, while the derailment of a moving train may have to be evaluated on a statistics basis. For this reason, the present formulation should be regarded as the one that serves to lay out the basic framework of the problem considered. Even though results have been computed for different cases, they should be regarded as a qualitative demonstration, rather than as a quantitative assessment.

2. ANALYSIS MODEL FOR TRAIN–RAIL–BRIDGE SYSTEM

Figure 1 depicts a train travelling with speed v over a simply supported bridge shaken by an earthquake. The train is assumed to consist of a series of separate identical cars, each of which consists of one car body, two bogies and four wheelsets, as shown in Figure 2, and has 27 degrees of freedom (d.o.f.) in total. By this model, the vertical, lateral, rolling, yawing and pitching motions of the car body as well as the vertical and lateral contact forces between the rail and the wheels can be simulated. The bridge is a box girder bridge with double tracks, i.e., Tracks A and B, each of which is simplified as a set of infinite, continuous twin rails lying on a single-layer ballast foundation, and the bridge structure is modelled as a 3-D Bernoulli–Euler beam (see Figure 2). As can be seen, the vehicle (i.e., train car), rails and bridge form a *train–bridge interaction* system, or more specifically, a *vehicle–rail–bridge interaction* (VRBI) system. The vehicle, track and bridge structures are all assumed to be linearly elastic during the earthquake excitation.

In this study, the car model Series 300 of Japan's Shinkansen (SKS) system [4] is adopted for the train car. The rails are assumed to be of the UIC-60 type and the bridge is of uniform

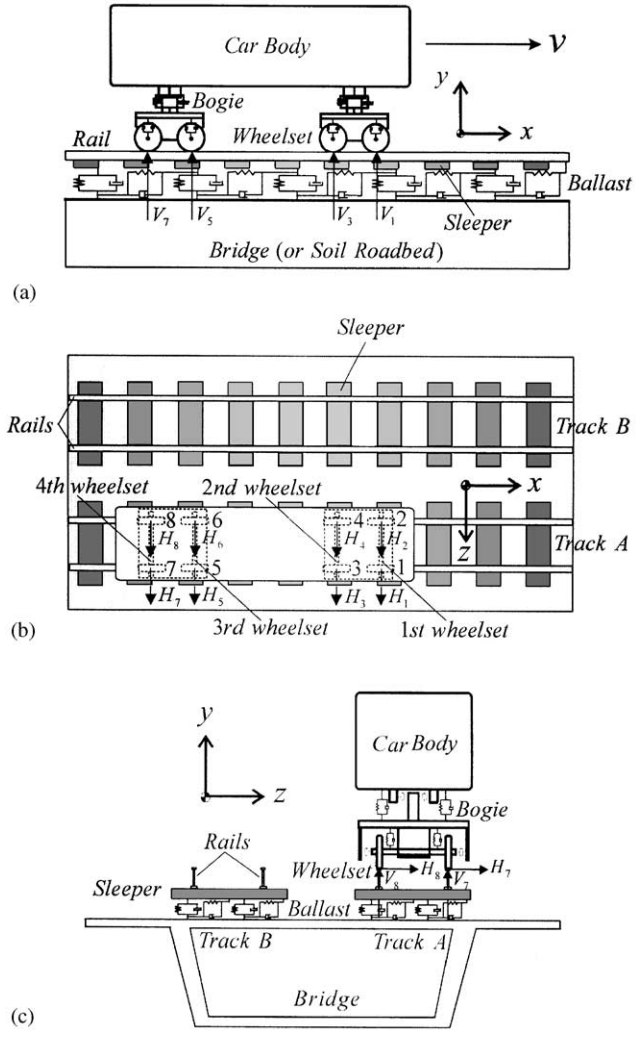

Figure 2. Train car, track and bridge models: (a) side view, (b) top view, and (c) rear view.

cross-sections. Some primary data for the vehicle, track and bridge models are listed in Table 1. More details for the models can be found in references [5, 6]. It should be noted that all the conclusions made in this paper remain strictly valid only for the particular models and assumptions adopted.

3. RAILWAY–BRIDGE SYSTEM WITH GROUND MOTIONS

In this section, focus is placed on inclusion of the ground-motion effects in each component of the railway–bridge system. As shown in Figure 1, three types of elements are conceived for the rails lying on the ballast layer represented as uniformly distributed spring–dashpot units, i.e., the *central finite rail* (CFR), *left semi-infinite rail* (LSR) and *right semi-infinite rail* (RSR) *elements*. The box-girder bridge is modelled by the conventional 3-D beam elements, each of which contains three translations and three rotations at each of the

TABLE 1

Some primary data for the vehicle, track and bridge

Item	Value
Vehicle	
Mass of the car body	41·75 t
Mass moment of inertia of the car body (about the z-axis)	2080 t m^2
Longitudinal distance between the two bogies	17·5 m
Mass of the bogie	3·04 t
Mass of the wheelset	1·78 t
Stiffness of the vertical primary suspension system	590 kN/m
Damping of the vertical primary suspension system	19·6 kN s/m
Stiffness of the lateral primary suspension system	2350 kN/m
Stiffness of the vertical secondary suspension system	265 kN/m
Damping of the vertical secondary suspension system	45·1 kN s/m
Stiffness of the lateral secondary suspension system	176 kN/m
Damping of the lateral secondary suspension system	39·2 kN s/m
Nominal radius of the wheel	0·455 m
Track	
Young's modulus of the rails	210 GPa
Per-unit-length mass of the rails (including the mass of the sleepers)	0·587 t/m
Sectional moment of inertia of the rails (about the z-axis)	$6{\cdot}12 \times 10^{-5}$ m^4
Per-unit-area vertical stiffness of the ballast	92·3 MN/m/m^2
Per-unit-area horizontal stiffness of the ballast	22·6 MN/m/m^2
Per-unit-area vertical and horizontal damping of the ballast	3·9 MN s/m/m^2
Gauge length	1·5 m
Bridge	
Young's modulus	28·25 GPa
Per-unit-length mass (including the mass of the ballast layer)	41·7 t/m
Per-unit-length mass moment of inertia (about the x-axis)	495 t m^2
Sectional area	6·73 m^2
Sectional moment of inertia (about the z-axis)	7·84 m^4
Sectional polar moment of inertia (about the x-axis)	15·65 m^4
Vertical distance between the deck and the center of torsion	1·2 m
Bridge span	30 m
Damping ratio (for the entire track–bridge system)	0·025

two end nodes. The equations of motion for the CFR, LSR, RSR and bridge elements derived in references [5, 6] will be extended to include the earthquake-induced effects. All the quantities associated with Tracks A, B, and the bridge will be denoted by symbols with subscripts "A", "B" and "b" respectively. For the sake of brevity, the derivations to follow will be made only for Track A. It is realized that the same procedure can be extended for Track B, as given in the Appendix A.

3.1. CENTRAL FINITE RAIL (CFR) ELEMENT

The two rails of Track A are lumped together and represented by a single line of twin-rail elements, lying on the ballast layer modelled as uniform spring–dashpot units. The twin rail element has two nodes, each of which has three translational and three rotational d.o.f.s. By the virtual work principle, the equation of equilibrium for the CFR element can be

written as

$$\int_0^l E_r A_r u'_A \delta u'_A \,\mathrm{d}\xi + \int_0^l E_r I_{rz} v''_A \delta v''_A \,\mathrm{d}\xi + \int_0^l E_r I_{ry} w''_A \delta w''_A \,\mathrm{d}\xi =$$

$$- \int_0^l m_r (\ddot{u}_A \delta u_A + \ddot{v}_A \delta v_A + \ddot{w}_A \delta w_A) \,\mathrm{d}\xi$$

$$- \int_0^l I_r^* \ddot{\theta}_A \delta\theta_A \,\mathrm{d}\xi - \int_0^l c_r (\dot{u}_A \delta u_A + \dot{v}_A \delta v_A + \dot{w}_A \delta w_A) \,\mathrm{d}\xi - \int_0^l c_r^* \dot{\theta}_A \,\mathrm{d}\xi$$

$$+ 2l_d \int_0^l [p_c(\xi) + p_k(\xi)]\, \delta u_A \,\mathrm{d}\xi + \int_0^l \int_{l_b - l_d}^{l_b + l_d} [q_c(\xi, z) + q_k(\xi, z)]\, [\delta v_A - (z - l_b)\, \delta\theta_A] \,\mathrm{d}z \,\mathrm{d}\xi$$

$$+ 2l_d \int_0^l [r_c(\xi) + r_k(\xi)]\, \delta w_A \,\mathrm{d}\xi + \langle \delta d_A \rangle \{f_A\}, \tag{1}$$

where the subscript "r" indicates the "rails", E_r is Young's modulus, A_r is the sectional area, I_{ry}, I_{rz} are the moment of inertia about the y-, and z-axis, m_r the per-unit-length mass (including mass of sleepers), I_r^* the per-unit-length mass moment of inertia about the x-axis (including that of sleepers), c_r, c_r^* the visco-damping coefficients, l_b the distance between the centreline of Track A and the bridge, l_d the half-length of sleepers, l the length of the twin-rail element; $\{d_A\}$ denotes the nodal displacement of the twin rail element, $\{f_A\}$ the corresponding external loads; u_A, v_A, w_A the displacements along the x-, y-, and z-axis; and θ_A the rotation about the x-axis of the twin-rail element. The interaction forces arising from the relative motion of the twin-rail and bridge elements, i.e., (p_c, p_k), (q_c, q_k) and (r_c, r_k), can be defined as

$$\begin{aligned}
&p_c(\xi) = c_{bh1}^*(\dot{u}_b(\xi) - \dot{u}_A(\xi)), \qquad p_k(\xi) = k_{bh1}^*(u_b(\xi) - u_A(\xi)),\\
&q_c(\xi, z) = c_{bv1}^*(\dot{v}_b(\xi) - z\dot{\theta}_b(\xi) - \dot{v}_A(\xi) + (z - l_b)\,\dot{\theta}_A(\xi)),\\
&q_k(\xi, z) = k_{bv1}^*(v_b(\xi) - z\theta_b(\xi) - v_A(\xi) + (z - l_b)\,\theta_A(\xi)),\\
&r_c(\xi) = c_{bh1}^*(\dot{w}_b(\xi) - h\dot{\theta}_b(\xi) - \dot{w}_A(\xi)),\\
&r_k(\xi) = k_{bh1}^*(w_b(\xi) - h\theta_b(\xi) - w_A(\xi)),
\end{aligned} \tag{2}$$

where c_{bh1}^*, k_{bh1}^* and c_{bv1}^*, k_{bv1}^*, respectively, denote the unit-area horizontal and vertical damping and stiffness coefficients of the ballast on the bridge; u_b, v_b, w_b the displacements along the three axes; and θ_b the rotation about the x-axis of the bridge element; h is the vertical distance between the deck and the centre of torsion of the bridge section. The longitudinal and lateral damping and stiffness coefficients of the ballast are assumed to be the same, denoted as c_{bh1}^* and k_{bh1}^*. The displacement fields of the twin-rail and bridge elements can be expressed in terms of the nodal d.o.f.s using linear or cubic Hermitian interpolation functions [7]. Substituting these displacement fields into equation (1) yields the equation of motion for the CFR element made up of twin rails for Track A that is free of any ground motions as

$$[m_A]\{\ddot{d}_A\} + [c_A]\{\dot{d}_A\} + [k_A]\{d_A\} = \{f_A\} + [c_{Ab}]\{\dot{d}_b\} + [k_{Ab}]\{d_b\}, \tag{3}$$

where $[m_A]$, $[c_A]$ and $[k_A]$ are the mass, damping and stiffness matrices of the twin-rail element, and $\{d_A\}$ the nodal displacement of the bridge element. The damping and stiffness matrices on the right-hand side of equation (3), i.e., $[c_{Ab}]$ and $[k_{Ab}]$, represent the interaction effects caused by the relative motion of the twin-rail and bridge elements through the inserted ballast layer represented as uniformly distributed spring–dashpot units. Details for the matrices and vectors involved in equation (3) are available in Appendix A.

For a railway bridge subjected to a ground motion, the terms $\{d_A\}$ and $\{d_b\}$ in equation (3) should be interpreted as the *total* or *absolute* displacements of the twin-rail and bridge elements. The total displacements of the bridge element $\{d_b\}$ can be divided into two parts:

$$\{d_b\} = \{d_b^n\} + \{d_b^r\}, \tag{4}$$

where $\{d_b^n\}$ denotes the natural deformations and $\{d_b^r\}$ the rigid displacements of the bridge element due to the ground motion. The latter can be determined as

$$\{d_b^r\} = [R]\{u_g\}, \tag{5}$$

where $[R]$ denotes the transformation matrix and $\{u_g\}$ the support displacements of the bridge due to the ground motion, which are prescribed in general. Based on the assumption that the support motions occur synchronously and that no rotations are induced by the ground motions on the support of the bridge, the transformation matrix $[R]$ can be given as

$$[R] = \begin{bmatrix} [r] \\ [r] \end{bmatrix}, \qquad [r] = \begin{bmatrix} [I]_{3\times 3} \\ [0]_{3\times 3} \end{bmatrix}, \tag{6}$$

where $[I]$ is a 3×3 unit matrix and $[0]$ a zero matrix. The support displacements $\{u_g\}$ are assumed to be 3-D,

$$\{u_g\} = \langle u_{gx} \;\; u_{gy} \;\; u_{gz} \rangle^{\mathrm{T}}, \tag{7}$$

where u_{gx}, u_{gy} and u_{gz} denote the displacement components along the three axes.

Substituting equations (4)–(7) into equation (3), one obtains the equation of motion for the CFR element with due account for the ground motion as

$$[m_A]\{\ddot{d}_A\} + [c_A]\{\dot{d}_A\} + [k_A]\{d_A\} = \{f_A^t\} + [c_{Ab}]\{\dot{d}_b^n\} + [k_{Ab}]\{d_b^n\}, \tag{8}$$

where $\{f_A^t\}$ denotes the total equivalent nodal forces of the element under the ground motion,

$$\begin{aligned} \{f_A^t\} &= \{f_A\} + \{f_A^c\} + \{f_A^k\} \\ &= \{f_A\} + \underline{[c_{Ab}][R]\{\dot{u}_g\}} + \underline{[k_{Ab}][R]\{u_g\}}. \end{aligned} \tag{9}$$

As can be seen, the parts of the equivalent nodal forces induced by ground motions, i.e., $\{f_A^c\}$ and $\{f_A^k\}$, relate to the displacement and velocity, but not acceleration, of the ground (or supports).

3.2. BRIDGE ELEMENT

The bridge element is the conventional 3-D solid beam element, with six d.o.f.s, at each node. Following the same procedure as that for the CFR element, the equation of motion

for the bridge element, considering the interaction with the twin-rail elements of the two tracks through the ballast layer, can be derived as

$$[m_b]\{\ddot{d}_b^n\} + [c_b]\{\dot{d}_b^n\} + [k_b]\{d_b^n\} = \{f_b^t\} + [c_{bA}]\{\dot{d}_A\} + [k_{bA}]\{d_A\} + [c_{bB}]\{\dot{d}_B\} + [k_{bB}]\{d_B\}, \tag{10}$$

where $\{d_b^n\}$ denotes the natural deformations of the bridge element, $\{d_A\}$ and $\{d_B\}$ the total displacements of the associated rail elements of Tracks A and B, $[m_b]$, $[c_b]$ and $[k_b]$ the mass, damping and stiffness matrices of the beam element, and $[c_{bA}]$, $[k_{bA}]$ and $[c_{bB}]$, $[k_{bB}]$ the damping and stiffness effects resulting from the interaction with the rail elements of Tracks A and B through the ballast layer. All these matrices are available in Appendix A. Note that due to the interaction between the twin-rail and bridge elements, the matrices $[c_{bA}]$ and $[k_{bA}]$ are identical to $[c_{Ab}]$ and $[k_{Ab}]$, respectively, that is, $[c_{bA}] = [c_{Ab}]$ and $[k_{bA}] = [k_{Ab}]$. Similarly, $[c_{bB}]$ and $[k_{bB}]$, respectively, are identical to $[c_{Bb}]$ and $[k_{Bb}]$. The total forces $\{f_b^t\}$ of the bridge element are

$$\begin{aligned}\{f_b^t\} &= \{f_b\} + \{f_b^m\} + \{f_b^c\} + \{f_b^k\} \\ &= \{f_b\} - \underline{[m_b][R][\ddot{u}_g]} - \underline{([c_{bA}] + [c_{bB}])[R]\{\dot{u}_g\}} + \underline{([k_{bA}] + [k_{bB}])[R]\{u_g\}},\end{aligned} \tag{11}$$

Here, $\{f_b^m\}$ represents the equivalent inertia forces due to the rigid motions of the bridge element caused by ground motions, and $\{f_b^c\}$ and $\{f_b^k\}$ the equivalent damping and restoring forces due to the restraint effect of the ballast layer beneath Tracks A and B relative to the bridge element under the ground motions. Evidently, the parts of nodal forces induced by ground motions on the bridge element relate not only to the acceleration, but also displacement and velocity of the ground.

3.3. LEFT SEMI-INFINITE RAIL (LSR) ELEMENT

Both the LSR and RSR elements are semi-infinite elements, each of which consists of only a single node at one end, with the other end extending to infinity represented by functions of decaying nature. Unlike the CFR element, both the LSR and RSR elements are directly affected by motion of the ground on which it lies. The equation of motion for the LSR element used to simulate Track A under the ground motion can be written as follows:

$$[m_l]\{\ddot{d}_{Al}\} + [c_l]\{\dot{d}_{Al}\} + [k_l]\{d_{Al}\} = \{f_{Al}^t\}, \tag{12}$$

where $\{d_{Al}\}$ denotes the nodal displacements of the element, which consists of three translations and three rotations at the starting node and $[m_l]$, $[c_l]$ and $[k_l]$ are the mass, damping and stiffness matrices of the LSR element, which are available in Appendix A. The total nodal forces $\{f_{Al}^t\}$ of the element, which consist of the loads directly acting on the node and the equivalent nodal forces due to ground motion, can be given as

$$\{f_{Al}^t\} = \{f_{Al}\} + \{f_{Al}^c\} + \{f_{Al}^k\}, \tag{13}$$

where $\{f_{Al}\}$ denotes the loads directly acting on the nodes, and $\{f_{Al}^c\}$ and $\{f_{Al}^k\}$ the forces induced by the ground motion

$$\{f_{Al}^c\} = 2l_d c_{bh2}^* \int_{-\infty}^{0} \dot{u}_{gx}\{N_u\}\,\mathrm{d}\xi + 2l_d c_{bv2}^* \int_{-\infty}^{0} \dot{u}_{gy}\{N_v\}\,\mathrm{d}\xi + 2l_d c_{bh2}^* \int_{-\infty}^{0} \dot{u}_{gz}\{N_w\}\,\mathrm{d}\xi,$$
$$\{f_{Al}^k\} = 2l_d k_{bh2}^* \int_{-\infty}^{0} u_{gx}\{N_u\}\,\mathrm{d}\xi + 2l_d k_{bv2}^* \int_{-\infty}^{0} u_{gy}\{N_v\}\,\mathrm{d}\xi + 2l_d k_{bh2}^* \int_{-\infty}^{0} u_{gz}\{N_w\}\,\mathrm{d}\xi, \tag{14}$$

where $\{N_u\}$, $\{N_v\}$ and $\{N_w\}$ denote the interpolation vectors for the LSR element in three directions which can be found in references [5, 6]; and c_{bh2}^*, k_{bh2}^* and c_{bv2}^*, k_{bv2}^* are the damping and stiffness coefficients of the ballast per unit area on the soil roadbed along the horizontal (h) and vertical (v) directions. Supposing that the ground displacement and velocity do not vary along the track, equation (14) can be rewritten as

$$\{f_{Al}^c\} = [c_{gl}]\{\dot{u}_g\} = [\{c_{glx}\} \quad \{c_{gly}\} \quad \{c_{glz}\}]\{\dot{u}_g\},$$
$$\{f_{Al}^k\} = [k_{gl}]\{u_g\} = [\{k_{glx}\} \quad \{k_{gly}\} \quad \{k_{glz}\}]\{u_g\}, \tag{15}$$

where

$$\{c_{glx}\} = \left\langle \frac{2l_d c_{bh2}^*}{\lambda_u} \quad 0 \quad 0 \quad 0 \quad 0 \quad 0 \right\rangle^{\mathrm{T}}, \qquad \{k_{glx}\} = \left\langle \frac{2l_d k_{bh2}^*}{\lambda_u} \quad 0 \quad 0 \quad 0 \quad 0 \quad 0 \right\rangle^{\mathrm{T}},$$
$$\{c_{gly}\} = \left\langle 0 \quad \frac{2l_d c_{bv2}^*}{\lambda_v} \quad 0 \quad 0 \quad 0 \quad \frac{-2l_d c_{bv2}^*}{2\lambda_v^2} \right\rangle^{\mathrm{T}},$$
$$\{k_{gly}\} = \left\langle 0 \quad \frac{2l_d k_{bv2}^*}{\lambda_v} \quad 0 \quad 0 \quad 0 \quad \frac{-2l_d k_{bv2}^*}{2\lambda_u^2} \right\rangle^{\mathrm{T}}, \tag{16}$$
$$\{c_{glx}\} = \left\langle 0 \quad 0 \quad \frac{2l_d c_{bh2}^*}{\lambda_w} \quad 0 \quad \frac{2l_d c_{bh2}^*}{2\lambda_w^2} \quad 0 \right\rangle^{\mathrm{T}},$$
$$\{k_{glz}\} = \left\langle 0 \quad 0 \quad \frac{2l_d k_{bh2}^*}{\lambda_w} \quad 0 \quad \frac{2l_d k_{bh2}^*}{2\lambda_w^2} \quad 0 \right\rangle^{\mathrm{T}},$$

where λ_u ,λ_v, λ_w denote the longitudinal, vertical and lateral characteristic numbers of the twin beam–Winkler foundation system, which have been defined in Appendix A.

3.4. RIGHT SEMI-INFINITE RAIL (RSR) ELEMENT

Following the same procedure for the LSR element, the equation of motion for the RSR element considering the ground motion for the two tracks can be derived:

$$[m_r]\{\ddot{d}_{Ar}\} + [c_r]\{\dot{d}_{Ar}\} + [k_r]\{d_{Ar}\} = \{f_{Ar}^t\}, \tag{17}$$

where $\{d_{Ar}\}$ denotes the nodal displacements and $[m_r]$, $[c_r]$ and $[k_r]$ are the mass, damping and stiffness matrices of the RSR element (see Appendix A). The total nodal forces $\{f_{Ar}^t\}$ of

the element are

$$\{f_{Ar}^t\} = \{f_{Ar}\} + \{f_{Ar}^c\} + \{f_{Ar}^k\},$$

$$\{f_{Ar}^c\} = [c_{gr}]\{\dot{u}_g\} = [\{c_{grx}\} \quad \{c_{gry}\} \quad \{c_{grz}\}]\{\dot{u}_g\}, \tag{18}$$

$$\{f_{Ar}^k\} = [k_{gr}]\{u_g\} = [\{k_{grx}\} \quad \{k_{gry}\} \quad \{k_{grz}\}]\{u_g\}$$

and $\{c_{grx}\} = \{c_{glx}\}$, $\{k_{grx}\} = \{k_{glx}\}$,

$$\{c_{gly}\} = \left\langle 0 \quad \frac{2l_d c_{bv2}^*}{\lambda_v} \quad 0 \quad 0 \quad 0 \quad \frac{2l_d c_{bv2}^*}{2\lambda_v^2} \right\rangle^{\mathrm{T}}, \quad \{k_{gry}\} = \left\langle 0 \quad \frac{2l_d k_{bv2}^*}{\lambda_v} \quad 0 \quad 0 \quad 0 \quad \frac{2l_d k_{bv2}^*}{2\lambda_v^2} \right\rangle^{\mathrm{T}},$$

$$\{c_{grx}\} = \left\langle 0 \quad 0 \quad \frac{2l_d c_{bh2}^*}{\lambda_w} \quad 0 \quad \frac{-2l_d c_{bh2}^*}{2\lambda_w^2} \quad 0 \right\rangle^{\mathrm{T}}, \tag{19}$$

$$\{k_{glz}\} = \left\langle 0 \quad 0 \quad \frac{2l_d k_{bh2}^*}{\lambda_w} \quad 0 \quad \frac{-2l_d k_{bh2}^*}{2\lambda_w^2} \quad 0 \right\rangle^{\mathrm{T}}.$$

As can be observed from the derivations presented in this section for the CFR, LSR, RSR and bridge elements, the inclusion of ground motions results only in addition of some earthquake-induced forces to the nodal forces, while the mass, damping and stiffness matrices remain the same as those for the case with no ground motions. Because of this, the earthquake-induced effects can be easily included in existing vehicle–bridge interaction analysis programs with no change on the system matrices. The only thing that should be done is to expand the vectors of nodal forces to include the earthquake-induced effects.

4. METHOD OF ANALYSIS

In the preceding section, focus has been placed on derivation of the equations of motion for each component of the railway–bridge system. By assembling the element matrices and vectors for all the components involved, the global matrices and vectors, as well as the equations of motion, for the railway–bridge or supporting system can be established. The railway–bridge system represents only one subsystem of the train–bridge system. The other subsystem is the moving train, consisting of a number of vehicles. In this study, the equations of motion for the moving train are constructed using the vehicle model presented in section 2, which have been formulated in references [5, 6] and will be skipped herein. The supporting and moving subsystems interact with each other through the *contact points* existing between the wheels and rails, as the train moves by. Clearly, the equations of motion for the two subsystems are *coupled* and *time dependent*.

For each train car, there are eight wheels, i.e., $i = 1$–8, and 16 contact forces, considering both the vertical and lateral components, i.e., $j = 1$–16. Using the Newmark-type finite-difference formulas and the constraint relation between the wheelset and the rails, one can first solve the equations of motion for each vehicle to obtain the vertical and lateral contact forces, i.e., V_i and H_i, in terms of the contact-point displacements d_{cj} and vehicle

forces $\tilde{p}_c$ and $\tilde{q}_c$ as [5, 6]

$$V_{i,t+\Delta t} = \tilde{p}_{c(2i-1),t+\Delta t} + \tilde{q}_{c(2i),t} + \sum_{j=1}^{16} (\tilde{m}_{c(2i-1)j}\,\ddot{d}_{cj,t+\Delta t} + \tilde{c}_{c(2i-1)j}\,\dot{d}_{cj,t+\Delta t} + \tilde{k}_{c(2i-1)j}\,d_{cj,t+\Delta t}), \tag{20}$$

$$H_{i,t+\Delta t} = \tilde{p}_{c(2i),t+\Delta t} + \tilde{q}_{c(2i),t} + \sum_{j=1}^{16} (\tilde{m}_{c(2i)j}\,\ddot{d}_{cj,t+\Delta t} + \tilde{c}_{c(2i)j}\,\dot{d}_{cj,t+\Delta t} + \tilde{k}_{c(2i)j}\,d_{cj,t+\Delta t}), \tag{21}$$

where $i = 1$–8, $j = 1$–16, and the matrices $[\tilde{m}_c]$, $[\tilde{c}_c]$, $[\tilde{k}_c]$ and vectors $\{\tilde{p}_c\}$, $\{\tilde{q}_c\}$ relate to the physical properties and wheel-load effects of the vehicle, as defined in references [5, 6].

By using the dynamic condensation technique developed in reference [8], the d.o.f.s of each of the moving vehicles can be condensed into the associated rail element(s) in contact to form the *vehicle–rail interaction* (VRI) element(s). By assembling all the VRI elements, the ordinary rail elements and the bridge elements, the equations of motion for the whole railway–bridge system can be established, which appear as second order differential equations. The Newmark-β integration method can then be called for to solve the system equations for each time step. Such an approach enables us to compute the vehicle response, contact forces and bridge response simultaneously. As was mentioned previously, the equations of motion for the twin-rail elements and bridge element considering the ground motion are identical to those for the case with no ground motions, except that the earthquake-induced forces should be included in the nodal forces for the present case. Consequently, the procedure presented in references [5, 6] for time–history analysis remains applicable herein for computing the response of the vehicle–bridge system shaken by earthquakes, if the earthquake-induced forces, which are functions of the acceleration, velocity and displacement of the ground motion, are duly updated at each incremental step.

5. DESCRIPTION OF INPUT EARTHQUAKE RECORDS

Four sets of ground accelerations induced by earthquakes are selected as the input excitation. The first two sets are for the 1940 El Centro and 1994 Northridge Earthquakes. The last two sets, i.e., TAP003 and TCU068, recorded at the freefield stations of Taipei and Taichung, respectively, during the 1999 Chi-Chi Earthquake in Taiwan, are used to simulate the *farfield* and *nearfault* excitations. The records for the El Centro and Northridge Earthquakes contain only a horizontal component of vibrations, while those for the Chi-Chi Earthquake contain both the EW horizontal and vertical components. In this study, the horizontal excitation of the earthquake is applied in the *lateral* (z) direction of the bridge for the sake of evaluating the stability of passing trains. Whenever the lateral ground motion is scaled down in terms of the PGA, the vertical ground motion is scaled down accordingly in the proportional manner.

As was stated previously, the seismic analysis of a train–railway system requires not only information on ground acceleration, but also on ground displacement and velocity as the input source. Since only ground accelerations were recorded for earthquakes, the ground velocity is integrated from the acceleration with baseline correction and Ormsby filtering for eliminating the lower frequencies, and the displacement integrated from the velocity with Ormsby filtering. The histograms of the ground motions computed for the EW and vertical components of the farfield station TAP003 have been plotted in Figures 3 and 4, and those of the nearfault station TCU068 in Figures 5 and 6. The histograms for the El Centro and Northridge Earthquakes are not shown since they are well known. Also

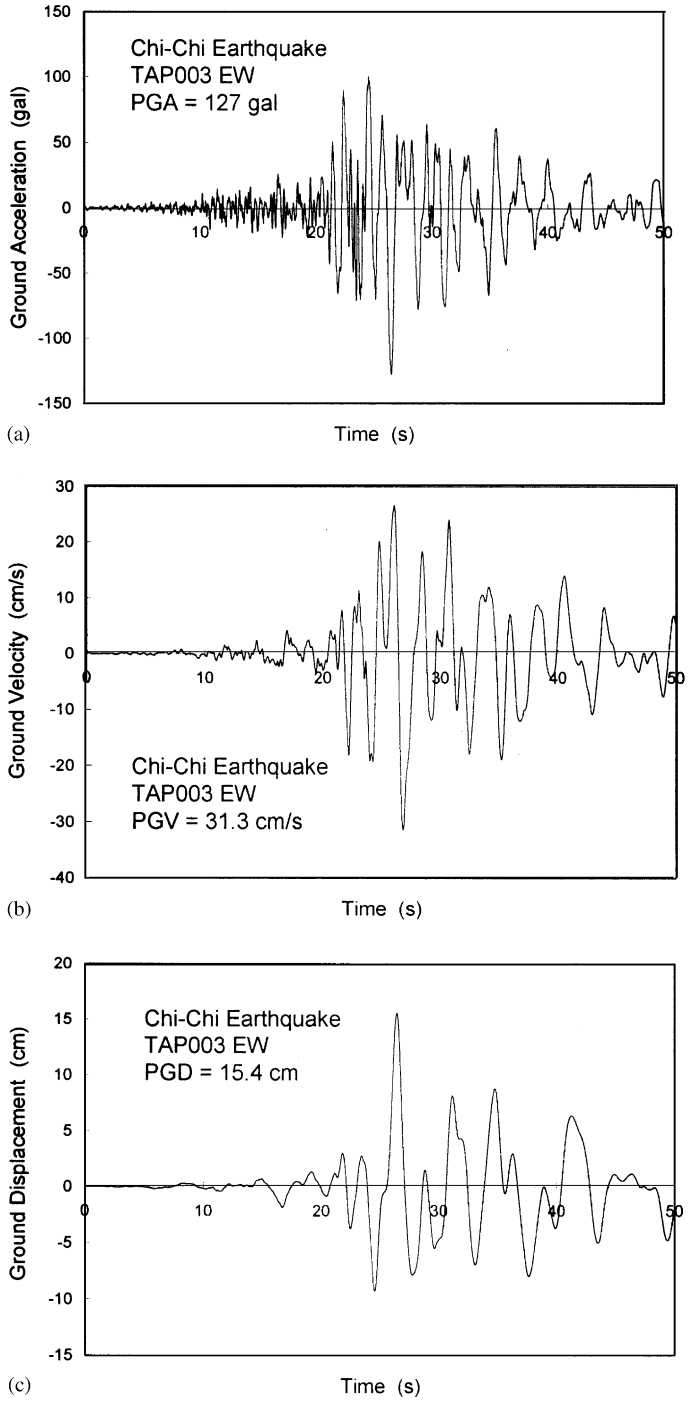

Figure 3. Lateral vibration response of the TAP003 ground motion of the Chi-Chi Earthquake: (a) acceleration, (b) velocity, and (c) displacement.

indicated in these figures are the peak ground acceleration (PGA), peak ground velocity (PGV) and peak ground displacement (PGD). The impulse-type vertical acceleration shown in Figure 6(a) is typical of a nearfault earthquake.

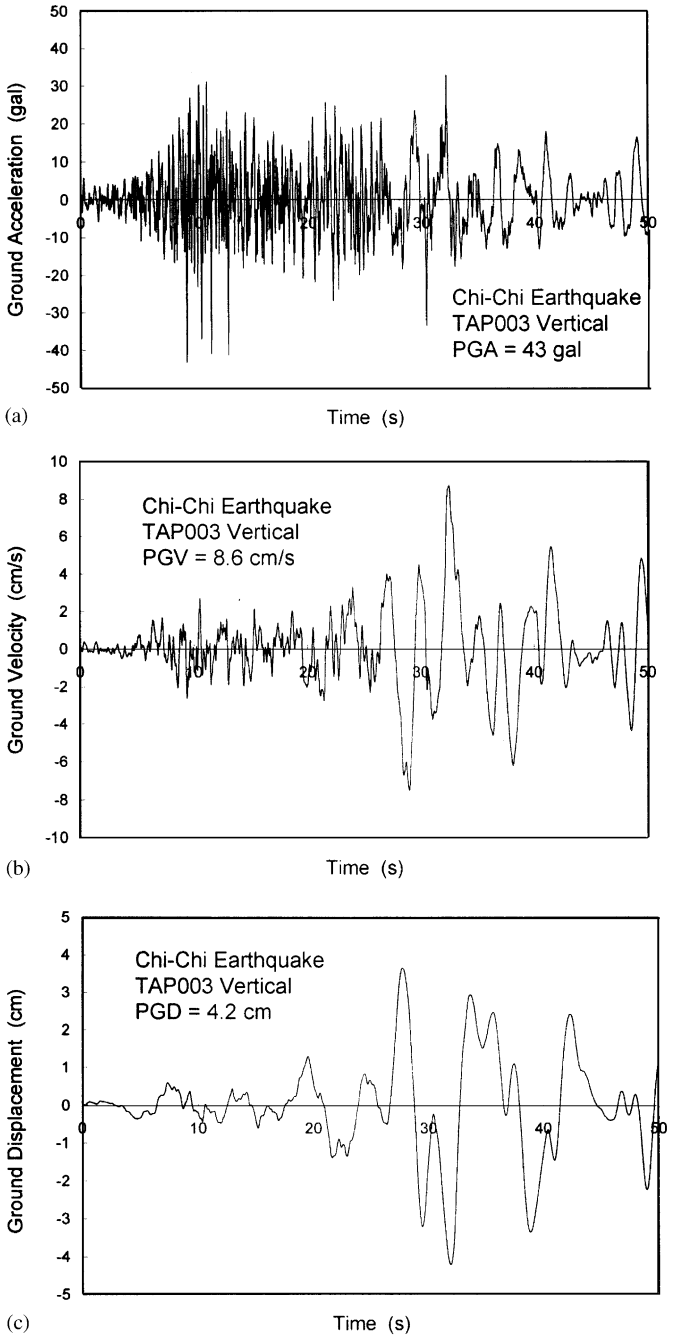

Figure 4. Vertical vibration response of the TAP003 ground motion of the Chi-Chi Earthquake: (a) acceleration, (b) velocity, and (c) displacement.

The ballast inserted between the rails and roadbed may display certain non-linear behaviour under severe ground motions, especially in the horizontal direction, which may affect the stability of moving trains, but has not been fully explored. According to Provision DS-804 of Germany [9], the horizontal resistance–relative displacement relation of the

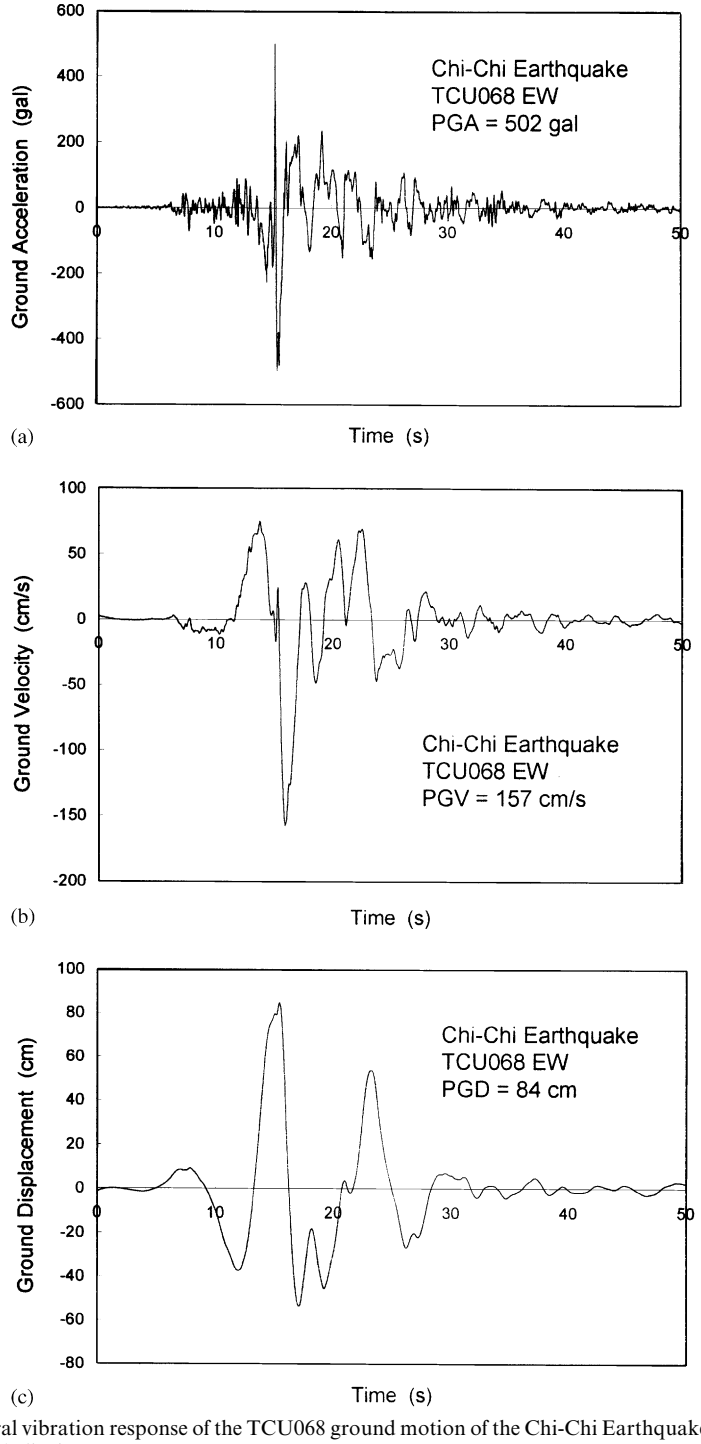

Figure 5. Lateral vibration response of the TCU068 ground motion of the Chi-Chi Earthquake: (a) acceleration, (b) velocity, and (c) displacement.

ballast can be approximately regarded as linear if the horizontal relative displacement of the ballast is less than 2 mm. For the four ground motions considered in the study, the maximum lateral relative displacement between the rails and the bridge caused by

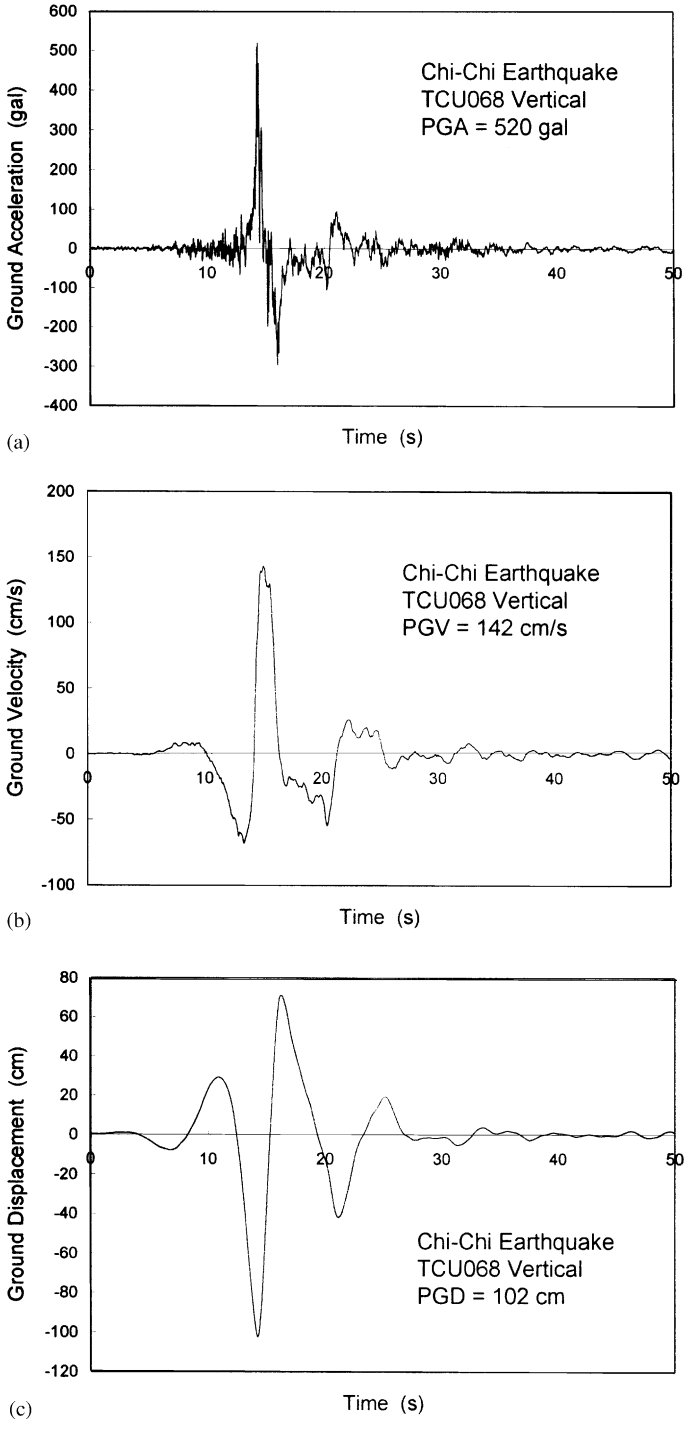

Figure 6. Vertical vibration response of the TCU068 ground motion of the Chi-Chi Earthquake: (a) acceleration, (b) velocity, and (c) displacement.

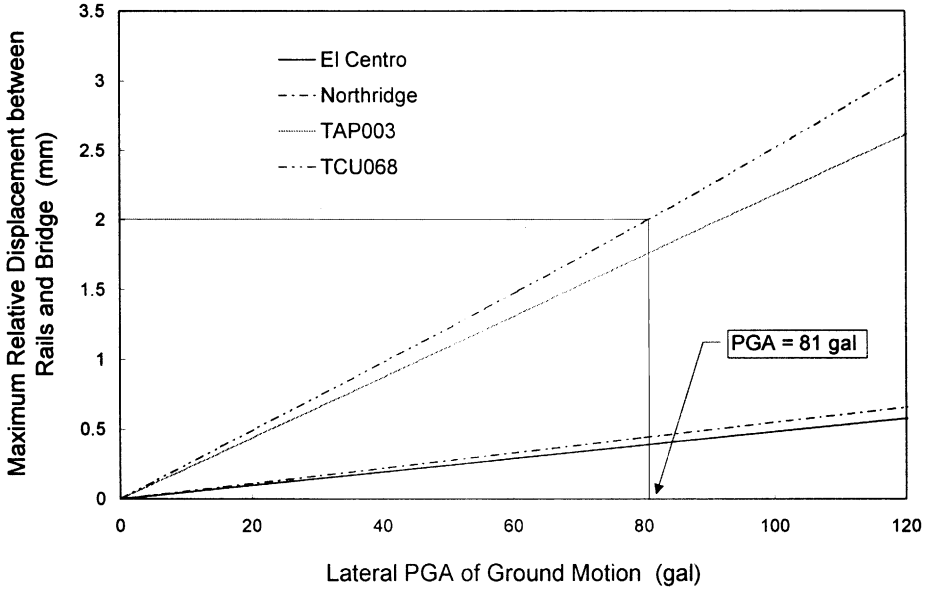

Figure 7. Maximum relative displacement of ballast under the action of the four ground motions.

the ground motion is less than 2 mm if the PGA is less than 80 gal, as shown in Figure 7. Further, it is quite possible that a well-designed bridge remains linearly elastic when subjected to ground motions with a PGA of up to 80 gal. For the reasons stated, as well as for simplification, the lateral PGAs of all the four ground motions will be limited to 80 gal, in order not to violate the assumption of linearity for tracks and structures.

6. TRAIN RESTING ON RAILWAY BRIDGE UNDER EARTHQUAKES

Throughout the numerical studies, the train is assumed to be of the SKS Series 300 type and will be represented by the model described in section 2. The time increment Δt used is 0·005 s, which is smaller than that used for recording the ground motions. It implies a frequency of $f = 1/\Delta t = 200$ Hz, higher than those implied by the wheels and rails. As a first test of the theory derived, we shall study the dynamic stability of a train car resting on a simply supported bridge of 30 m in length shaken by the four earthquakes considered. The primary data used for the train car, track and bridge have been listed in Table 1. The car is assumed to remain stationary on Track A of the bridge with its first wheelset located at the position $x = 25$ m prior to the earthquake. As was stated, all the four ground motions are normalized to have a lateral PGA of 80 gal.

6.1. CONTACT FORCES BETWEEN WHEELS AND RAILS

The vertical and lateral contact forces induced by the four excitations between the wheelsets and rails have been shown in Figure 8(a–d), in which only the contact forces for the first and second wheels of the first wheelset of the car shown in Figure 2(b) are presented. As can be seen, the vertical contact forces of the two wheels oscillate and cross each other during the earthquake. The oscillation appears to be most severe for the TAP003 excitation

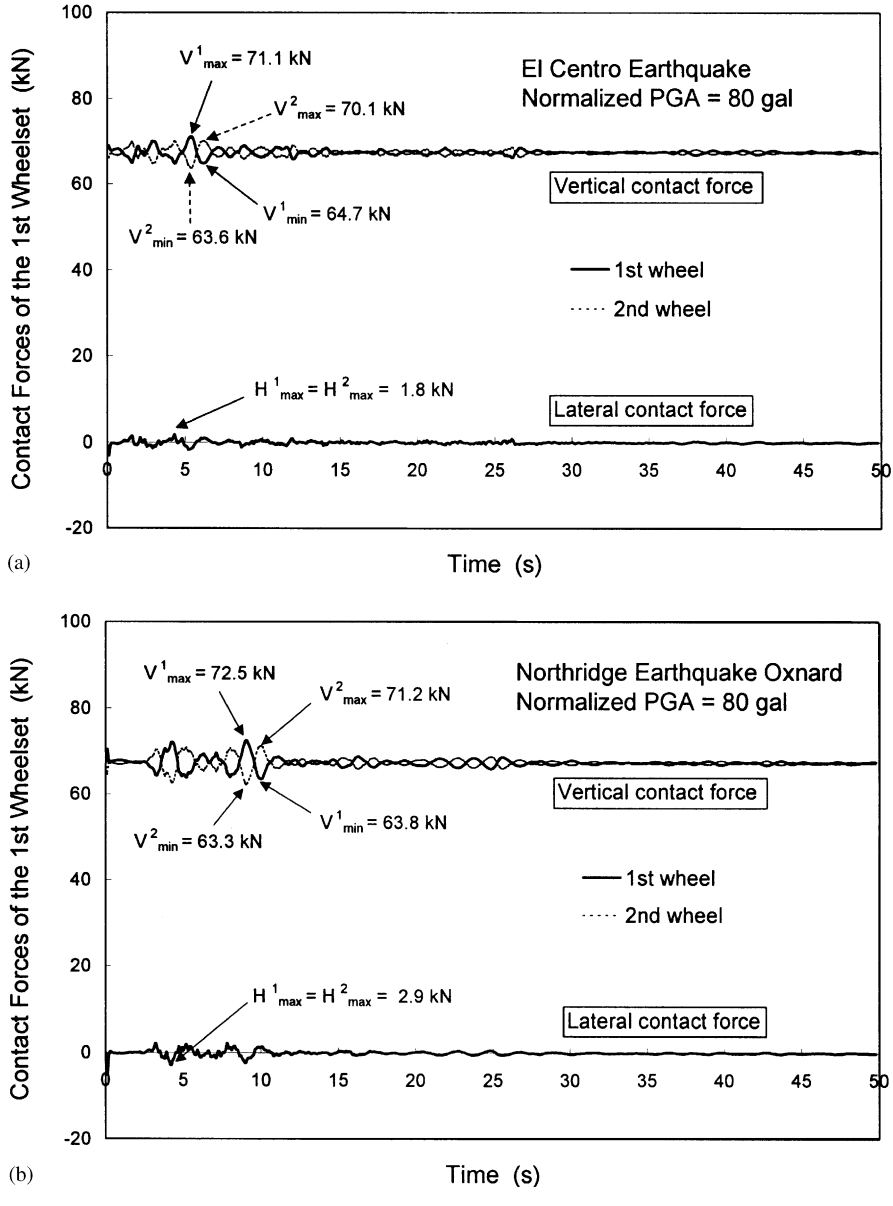

Figure 8. Contact forces of the first wheelset of the train car: (a) El Centro, (b) Northridge, (c) TAP003, and (d) TCU068 ground motions.

(see Figure 8(c)), where the vertical contact force of the first wheel reaches a maximum of 77·6 kN and a minimum of 57·4 kN, and that of the second wheel reaches a maximum of 77·3 kN and a minimum of 58·0 kN, implying a fluctuation of 30 and 29 per cents, respectively, with respect to a static axle load of 67 kN sustained by one wheel. The crossing behaviour of the two wheels of the first wheelset in each figure is an indication of the occurrence of *rolling motion* during the earthquake, which is harmful to the stability of the train car. Factors that may affect the contact forces of the car during the earthquake include the suspension stiffness of the car, the lateral–torsional stiffness of the bridge, the intensity

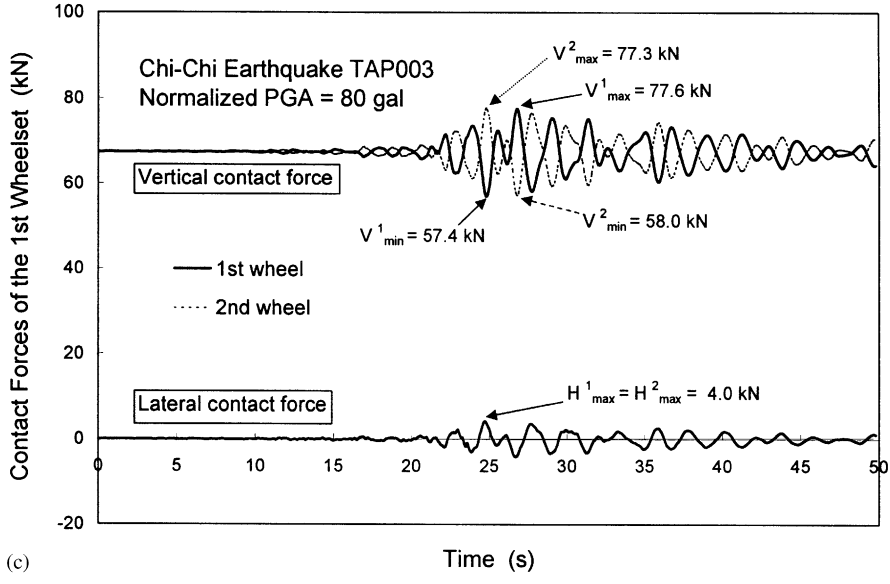

(c)

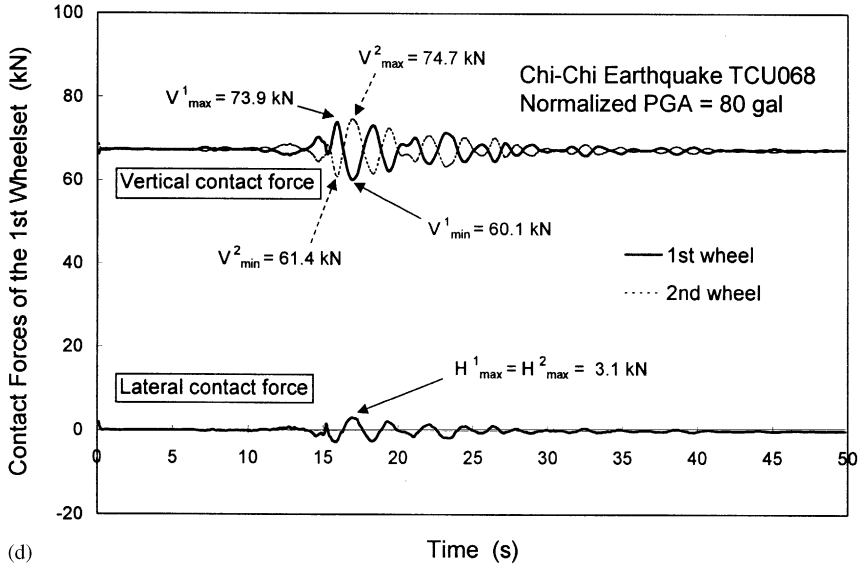

(d)

Figure 8. Continued

(PGA) and frequency intent of the earthquake. It should be added that the fourth wheelset shows the same behaviour as that of the first wheelset due to symmetry, and that similar, but smaller, rolling responses exist for the second and third wheelsets, which are not shown.

6.2. MAXIMUM YQ RATIO FOR WHEELSETS IN EARTHQUAKE

The *wheelset lateral to vertical force ratio*, referred to as the YQ ratio is adopted herein as an index for evaluating the stability of a train car resting on railway bridges shaken by earthquakes. This parameter is defined as $(YQ)_i = |H_{(2i-1)}/V_{(2i-1)}| + |H_{(2i)}/V_{(2i)}|$, where

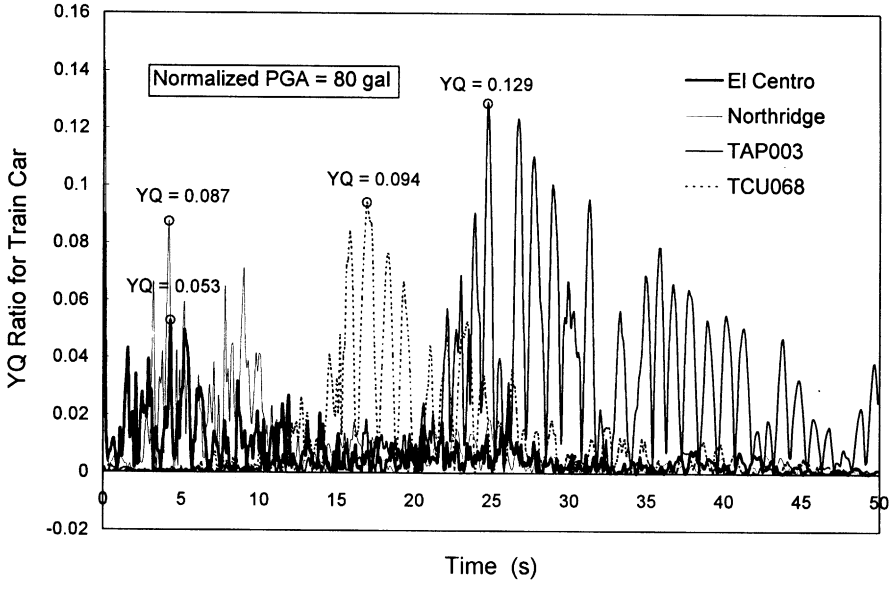

Figure 9. Time–history of the YQ ratio for the train car.

$i = 1, 2, 3$ or 4 for each of the four wheelsets (see Figure 2(b)), and H_j and V_j, with $j = 1$–8, respectively, denote the lateral and vertical contact forces acting on a wheel (also see Figure 2(b)). If $V_j \leqslant 0$, the jth wheel encounters the *jump* condition, and the wheelset to which the jth wheel belongs is at a high risk of derailment. To prevent the wheelset from derailment, an upper limit must be set on the YQ ratio. However, the determination of the stability limit is not easy, which requires more analytical and experimental investigations. In this study, a value of $YQ = 1{\cdot}5$ is set for the wheelset to remain *stable*, with no potential of derailment [10]. According to references [3, 10], a wheel will be safe and free of derailment (wheel climb), if the lateral (H) to vertical (V) force ratio (SYQ ratio) for the wheel does not exceed 1·0, namely, if $SYQ = |H/V| \leqslant 1{\cdot}0$. Based on the above considerations, there exists a transition zone from $YQ = 1{\cdot}5$–$2{\cdot}0$, where a wheelset will be at a high potential of derailment. This transition zone will be referred to as the *possible derailment zone* in this study. For the case when the YQ value computed is larger than 2·0 or $V \leqslant 0$, which implies the occurrence of derailment or jump with the wheelset, it will be regarded as the condition of *derailment*. Accordingly, the YQ value will be automatically set to 2·0, to distinguish it from the other two cases in the figures. Note that the actual derailment of a wheelset depends not only on the magnitude of the YQ ratio of the wheelset, but also on the lasting time of the YQ ratio exceeding the safety limit. Thus, it is conservative to assess the derailment potential of a wheelset using only the YQ ratio, as is done in this study, and to assess the stability of a train (car) using the maximum YQ ratios computed for all the wheelsets of the train (car).

Figure 9 shows the time–history plot of the maximum YQ ratio for the four wheelsets of the train car under the four ground motions. As can be seen, the peak YQ ratio computed for the TAP003 excitation is larger than those for the other three ones, which is similar to the contact force case depicted in section 6.1. In addition, the YQ ratios computed for the TAP003 and TCU068 excitations are generally larger than those for the El Centro and Northridge earthquakes. It can be observed that all the YQ ratios computed for all the four excitations fall well below the safety limit of 1·5, indicating that the four wheelsets of the

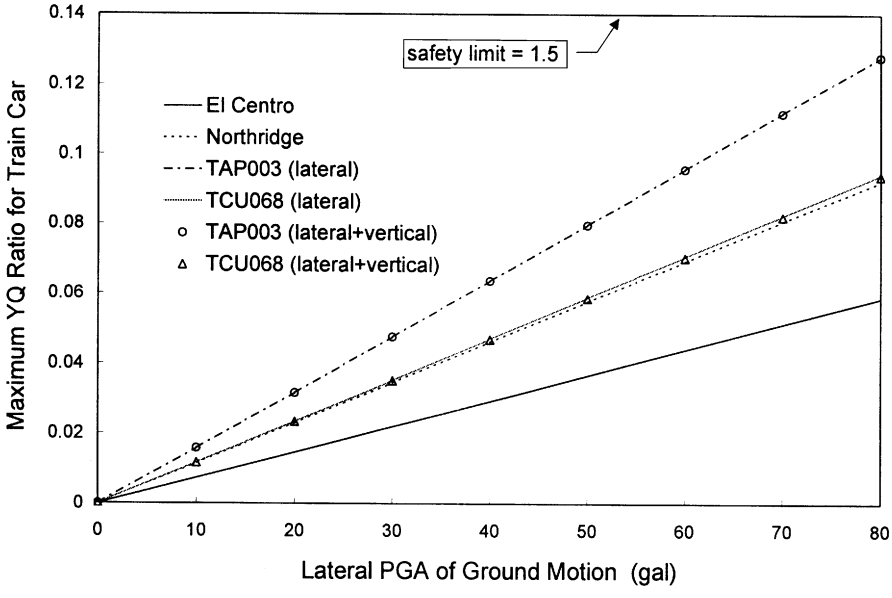

Figure 10. Maximum YQ ratio for the train car versus lateral PGA of the ground motion.

train car do not exhibit any instability during the ground motions. Therefore, it is concluded that a train initially at rest on the bridge will remain stable for the four earthquakes with a PGA of 80 gal, as long as the bridge does not experience any inelastic deformation. Here, one should not forget that the PGA level is generally higher for a nearfault motion than for a farfield motion.

6.3. STABILITY OF AN IDLE TRAIN UNDER EARTHQUAKES WITH VARIOUS INTENSITIES

The railway engineers may be interested in under what PGA level of excitation, an initially idle train car begins to lose its stability. For the case of lateral excitations only, the maximum YQ ratios computed for the wheelsets of the train car under the four target ground motions with various PGAs have been drawn in Figure 10. As can be seen, the maximum YQ ratios computed for the four excitations increase in proportion to the lateral PGA of the ground motion. Besides, the maximum YQ ratios for all range of the PGAs considered, i.e., up to 80 gal, are much less than the allowable limit of 1·5, indicating that the wheelsets of the car would not exhibit any instability or derailment under the specified ground motions if the lateral PGA does not exceed 80 gal. Of interest is the fact that the YQ ratio for the TAP003 motion is the largest among the four ground motions of the same PGA, implying that the TAP003 motion is more detrimental to stability of the train car than the other three, given the same PGA level.

For the case of *simultaneous* lateral and vertical excitations, the maximum YQ ratios computed for the train car under the TAP003 and TCU068 ground motions have also been shown in Figure 10, with the PGA of the vertical motion assumed to be proportional to that of the lateral one. As can be seen, the maximum YQ ratio for the train car due to action of both the lateral and vertical motions is nearly the same as that due to the lateral motion only, indicating that the vertical ground motion has little influence on the stability of trains initially resting on a railway bridge. An interpretation for this is that the vertical damping

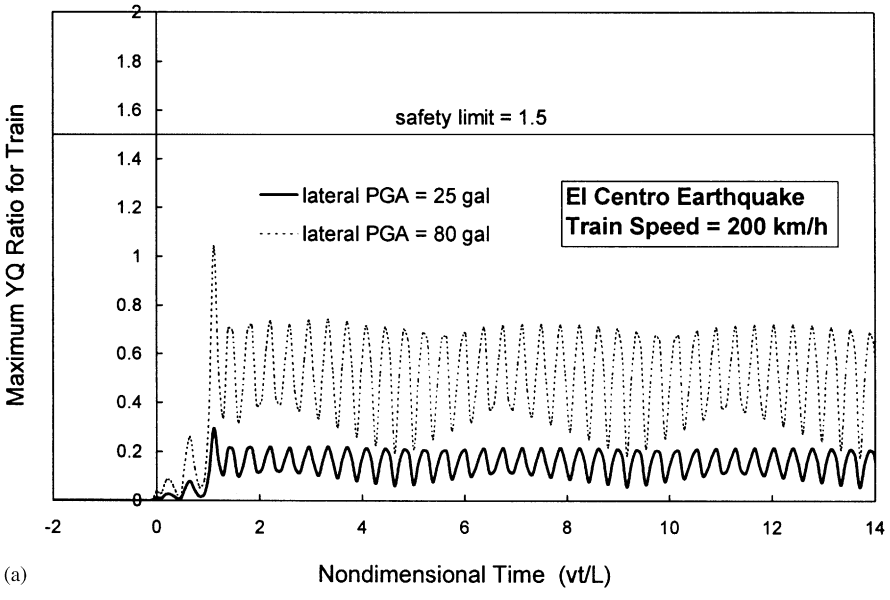

(a)

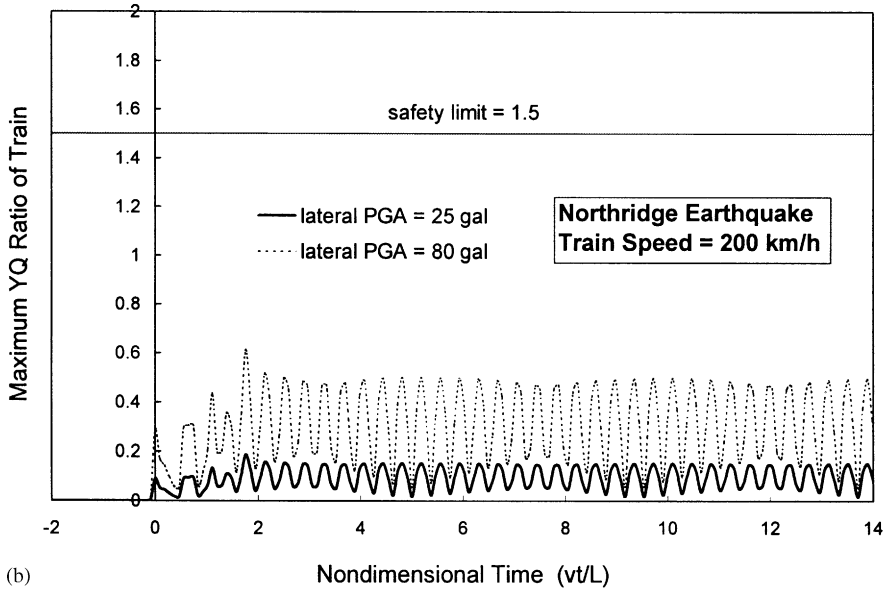

(b)

Figure 11. *YQ* ratio for the first wheelset of the first car of the train: (a) El Centro, (b) Northridge, (c) TAP003, and (d) TCU068 ground motions.

mechanism of the car is given sufficient time to dissipate the vibrational energy, since the car "stays" on the bridge. The same is not true for cars in travelling, due to the relatively short acting time.

7. TRAINS MOVING OVER RAILWAY BRIDGES UNDER EARTHQUAKES

In this section, we shall study the stability of a train travelling over a bridge shaken by earthquakes. The train is assumed to consist of 15 identical train cars. The same bridge and

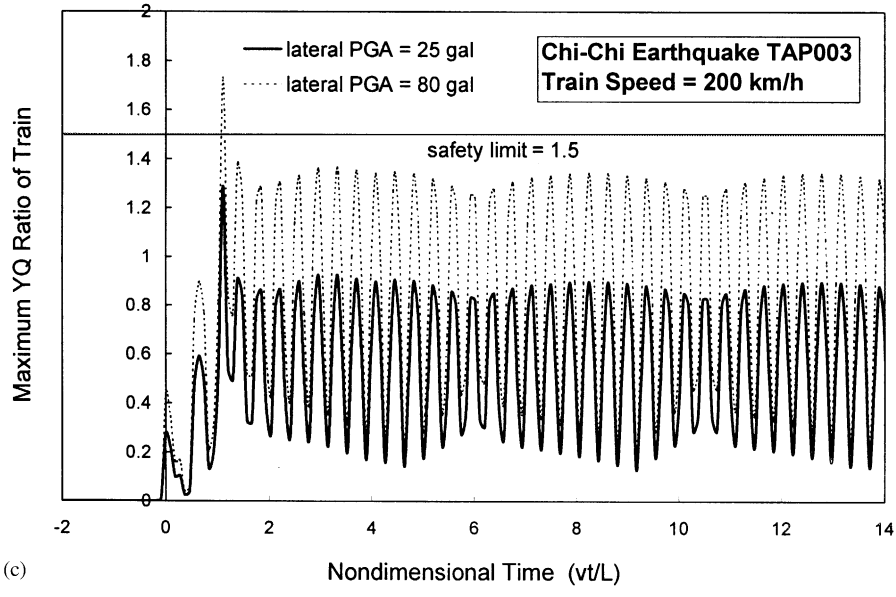

(c)

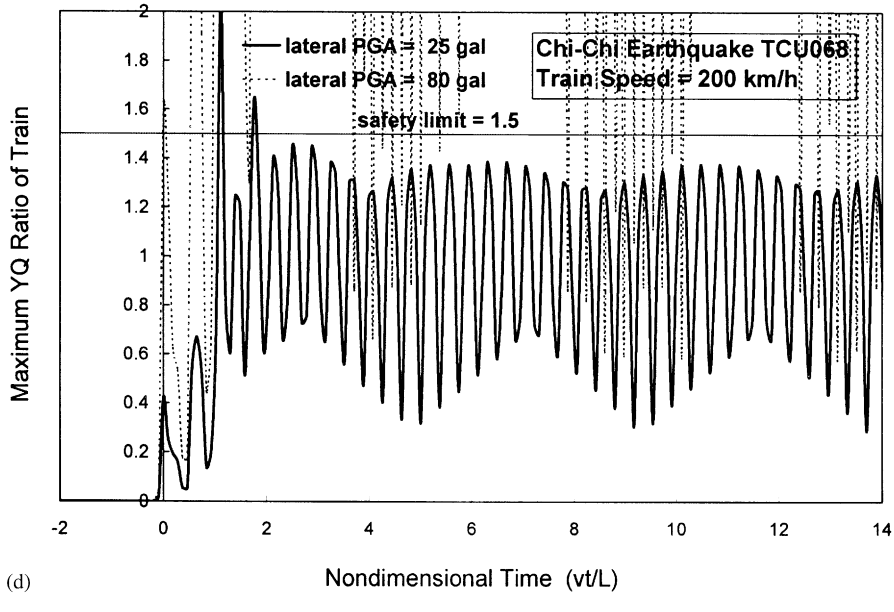

(d)

Figure 11. Continued

car models, as well as the four ground motions, specified in the preceding section are adopted.

7.1. MAXIMUM YQ RATIO FOR MOVING TRAINS IN EARTHQUAKE

For the case of *uni-directional* (i.e., lateral) excitation, the train is assumed to pass through the bridge at a speed of 200 km/h (= 55·6 m/s). Also, the bridge supports are assumed to be excited laterally by the earthquake exactly at the instant when the train enters the bridge.

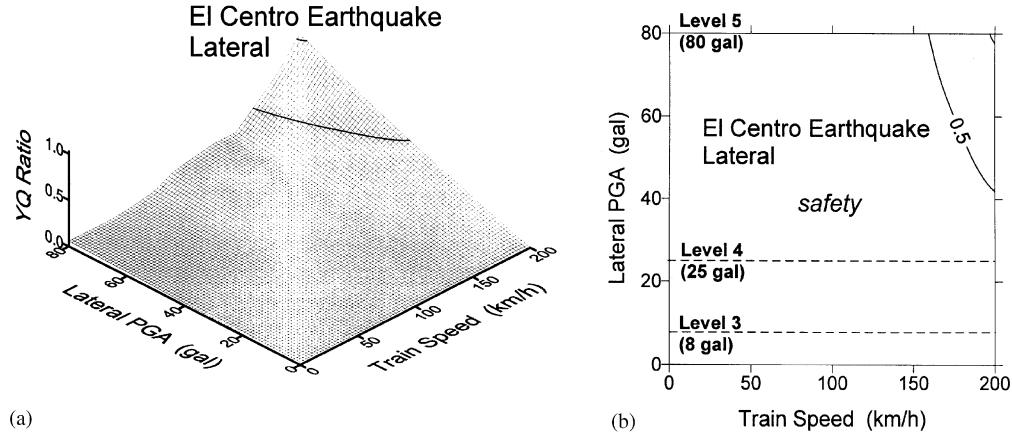

Figure 12. (a) Train speed–YQ ratio–lateral PGA plot. (b) Safety boundary for the train under the El Centro ground motion.

The maximum YQ ratios computed for the whole train moving over the bridge subjected to the four specified excitations with PGAs of 80 and 25 gal have been plotted in Figures 11(a–d). As can be seen from the case with PGA = 80 gal, the maximum YQ ratio for TCU068 exceeds evidently the stability limit of 1·5, indicating that derailment may occur in *nearfault* areas, while the maximum YQ ratios for the other three excitations are far below (for El centro and Northridge) or nearly equal to (for TAP003) the stability limit. In contrast, for the PGA of 25 gal, the maximum YQ ratios for the four ground motions are well below (for El Centro, Northridge and TAP003) or just slightly larger than (for TCU068) the stability limit of 1·5, indicating that generally no derailment may occur with the train under the action of the four ground motions with the PGA specified.

7.2. STABILITY ASSESSMENT OF MOVING TRAINS IN EARTHQUAKE

In earthquake-prone regions, it is important to assess the stability of trains running over bridges under the earthquake shaking. For *uni-directional* (i.e., lateral) excitations, the maximum YQ ratios computed for the *whole train* under the El Centro excitation with different PGAs (up to 80 gal) have been plotted with respect to the train speed (up to 200 km/h) in Figure 12. As can be seen, the values of 1·5 and 2·0 were also imposed (see the vertical axis of Figure 12(a)) to characterize the *safety* (with maximum YQ ratio $\leqslant 1{\cdot}5$), *possible instability* (with $1{\cdot}5 <$ maximum YQ ratio $\leqslant 2{\cdot}0$) and *instability* (with maximum YQ ratio $> 2{\cdot}0$) regions for the train. Similarly, the maximum YQ ratios computed for the Northridge, TAP003 and TCU068 excitations with different PGAs have been plotted with respect to the train speed in Figures 13–15, with the different regions of stability identified in part (b) of the figures. In all these figures, the PGA values of 8 and 25 gal have been referred to as seismic zones of Levels 3 and 4, respectively, according to the Taiwan codes.

The following observations can be made from Figures 12–15: (1) The maximum allowable speeds for stable running of the train are higher for smaller PGAs and lower for larger PGAs. (2) The ranges for stable running of the train under TAP003 and TCU068 are much narrower than those for the other two excitations, indicating that the train has a higher risk of derailment or instability when travelling over the bridge under the Chi-Chi Earthquake. (3) The train can move safely under El Centro and Northridge for all the speeds and PGAs considered. (4) If the lateral PGA of TAP003 is less than 30 gal, the train can cross the

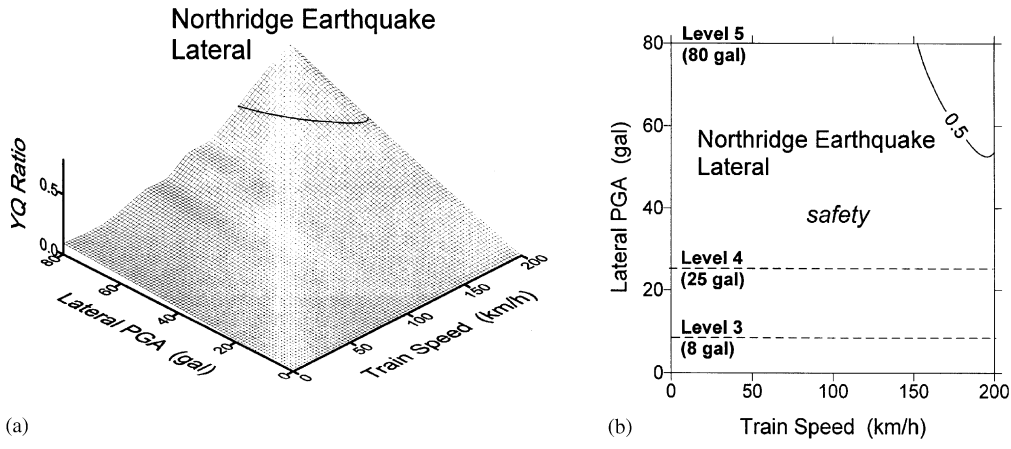

Figure 13. (a) Train speed–YQ ratio–lateral PGA plot. (b) Safety boundary for the train under the Northridge ground motion.

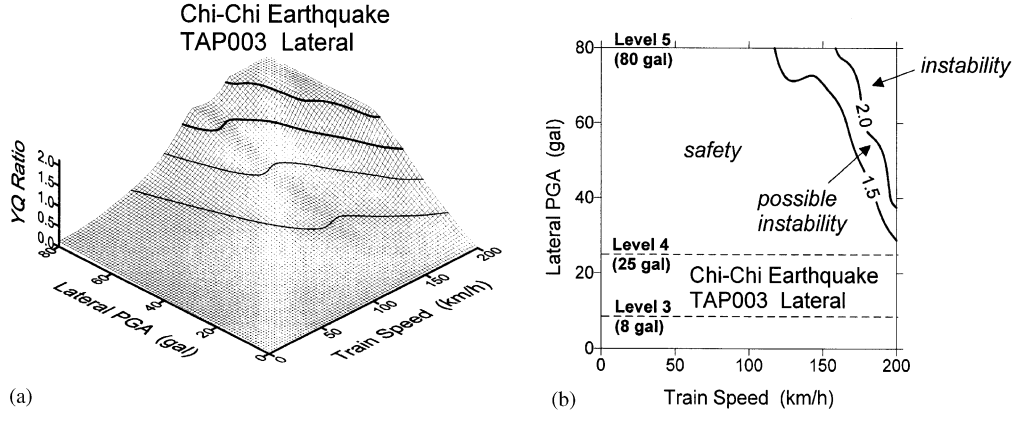

Figure 14. (a) Train speed–YQ ratio–lateral PGA plot. (b) Safety boundary for the train under the TAP003 ground motion (lateral only).

bridge safely at a speed of up to 200 km/h. The same is true for TCU068 if the PGA is less than 18 gal. (5) The train can move safely over the bridge without encountering any instability or derailment under TAP003 and TCU068 with a lateral PGA of up to 80 gal, if the train speed is kept below 122 and 85 km/h respectively.

For *bi-directional* (i.e., lateral and vertical) excitations, the results obtained for the TAP003 and TCU068 motions have been plotted in Figures 16 and 17 respectively. As can be seen, for the TAP003 motion, the maximum allowable speeds for the train under bi-directional excitations are nearly the same as those for uni-directional excitation. In contrast, for the TCU068 motion, the maximum allowable speeds for the train under bi-directional excitations are significantly less than those under uni-directional excitation. This can be attributed to the fact that the vertical PGA for the farfield (TAP003) motion is very small, i.e., 27 gal, compared with the lateral PGA of 80 gal (normalized), while that for the nearfault (TCU068) motion is rather high, i.e., 83 gal, compared with the same lateral PGA. In general, the presence of vertical excitation can drastically reduce the stability region or the maximum allowable speed for the train under a specific intensity (PGA).

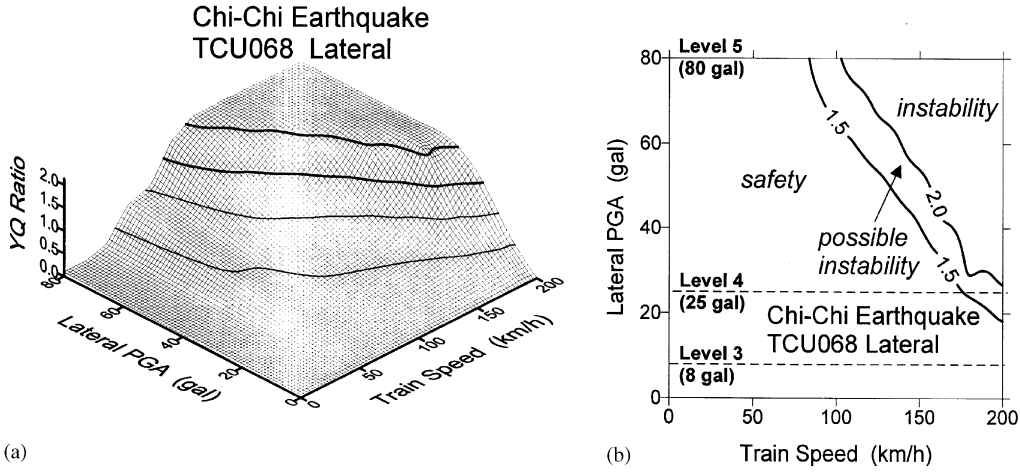

Figure 15. (a) Train speed–YQ ratio–lateral PGA plot. (b) Safety boundary for the train under the TCU068 ground motion (lateral only).

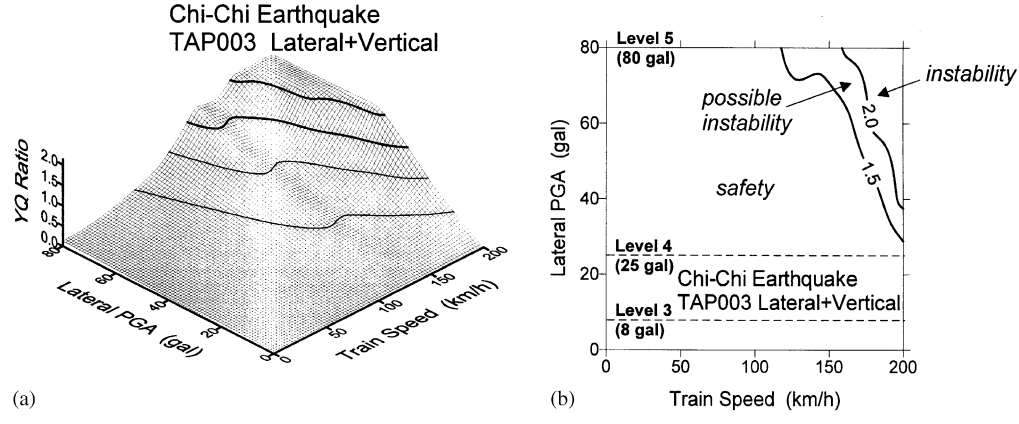

Figure 16. (a) Train speed–YQ ratio–lateral PGA plot, (b) safety boundary for the train under the TAP003 ground motion (lateral + vertical).

It should be noted that if the maximum YQ ratios for all the wheelsets of the train fall into the possible instability or instability regions, it does not necessarily mean that the train will really encounter overall derailment or instability. One reason for this is that the stability limits imposed on the YQ ratio are generally conservative due to consideration of safety. Another reason is that even though the YQ ratio of a single wheelset may exceed the safety limit, it still requires some time for derailment to develop, due to the linking action of the other parts of the car or the whole train. Further study is required in this regard to investigate the development of derailment and mechanism involved taking into account the linking effect of all the train cars.

8. CONCLUSIONS

The dynamic stability of trains moving over bridges shaken by earthquakes was investigated. The equations of motion for the train–rail–bridge system were first generalized

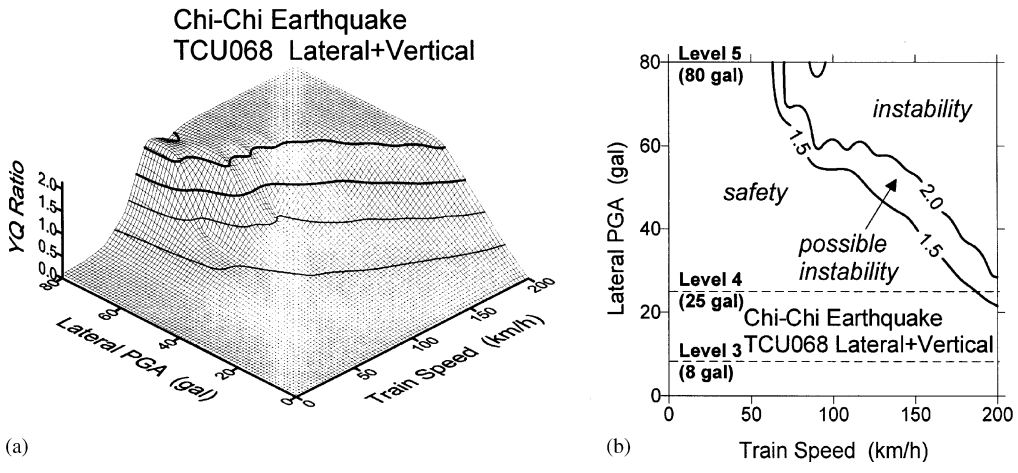

Figure 17. (a) Train speed–YQ ratio–lateral PGA plot. (b) Safety boundary for the train under the TCU068 ground motion (lateral + vertical).

to include the effects of ground excitations, resulting in some nodal force terms related not only to the acceleration, but also velocity and displacement of the ground. Since the generalized system equations are identical in form to those with no ground motions, the analysis procedure established previously for dealing with the train–bridge interactions can directly be adopted, with modifications made only for the nodal forces to include the earthquake-induced effects.

The following conclusions remain strictly valid only for the conditions set in the numerical studies: (1) A train car initially resting on the bridge remains safe under the four ground motions specified, up to a PGA level of 80 gal, assuming that no inelastic deformation occurs on the bridge and ballast. (2) As for the train to move safely over the bridge, the speed should be kept below the allowable speed computed for each excitation based on the YQ criterion. (3) The property of ground motions and the presence of vertical excitations affect drastically the stability of the moving train, especially for nearfault excitations, as represented by the TCU068 record. (4) Various regions of stability have been established for the train under the four ground motions.

This study represents only parts of a preliminary attempt to deal with the seismic effects on train–rail–bridge interactions. Further study should be carried out to consider the effect of more severe earthquakes, say, with a PGA larger than 80 gal, and to include more representative ground motions, as well as more precise criteria for derailment.

ACKNOWLEDGMENTS

The research reported herein was sponsored in part by the National Science Council of the ROC through Grant nos. NSC 89-2211-E-002-113 and NSC 89-2211-E-002-122.

REFERENCES

1. S. MIURA 1996 *Qualerly of RTRI* **37**, 139–147. Deformation of track and safety of train in earthquake.
2. T. MIYAMOTO, H. ISHIDA and M. MATSUO 1997 *Qualerly of RTRI* **38**, 117–122. Running safety of railway vehicle as earthquake occurs.

3. K. Q. MA and J. L. ZHU 1998 *Journal of Shanghai Tiedao University* **19**, 29–36. Seismic responses analysis for a system of high-speed train and continuous rigid-frame bridge.
4. H. WAKUI, N. MATSUMOTO, A. MATSUURA, and M. TANABE 1995 *Journal of Structural Mechanics and Earthquake Engineering* **513**, 129–138. Dynamic interaction analysis for railway vehicles and structures (in Japanese).
5. Y. S. WU 2000. *Ph.D. Thesis, Department of Civil Engineering, National Taiwan University, Taipei, Taiwan, R.O.C.* Dynamic interactions of train–rail–bridge system under normal and seismic conditions.
6. Y. S. WU, Y. B. YANG and J. D. YAU 2001 *International Journal of Vehicle Mechanics & Mobility* Three-dimensional analysis of train–rail–bridge interaction problems, to appear.
7. M. PAZ 1985 *Structural Dynamics Theory and Computation.* New York: Van Norstrand Reinhold Company, Inc.; second edition.
8. Y. B. YANG and Y. S. WU 2001 *Engineering Structures* **23,** 452–469. A versatile element for analysing vehicle–bridge interaction.
9. DEUTSCHE BUNDESBAHN 1993. DS804—Vorschrift fur Eisenbahnbrucken und sonstige Ingenieurbauwerke (VEI).
10. J. A. ELKINS and A. CARTER 1993 *Vehicle System Dynamics* **22**, 185–208. Testing and analysis techniques for safety assessment of rail vehicles: the state-of-the-art.

APPENDIX A

The following is a summary of the equations for the elements of Track B under ground motions.

(a) *CFR element*

Equation of motion:

$$[m_{tB}]\{\ddot{d}_{tB}\} + [c_{tB}]\{\dot{d}_{tB}\} + [k_{tB}]\{d_{tB}\} = \{f^t_{tB}\} + [c_{Bb}]\{\dot{d}^n_b\} + [k_{Bb}]\{d^n_b\}, \tag{A1}$$

where

$$\{f^t_B\} = \{f_B\} + \{f^c_B\} + \{f^k_B\} = \{f_B\} + \underline{[c_{Bb}][R]\{\dot{u}_g\}} + \underline{[k_{Bb}][R]\{u_g\}}. \tag{A2}$$

Based on the assumption that no rocking motion are induced by the earthquake on the bridge, the extra equivalent nodal forces induced by ground motions on the CFR element for Tracks A and B should be the same, namely,

$$\{f^c_B\} = \{f^c_A\}, \qquad \{f^k_B\} = \{f^k_A\}. \tag{A3}$$

The same results can be obtained for the two tracks through manipulation of the triple products in equation (9) involving the matrices $[c_{Ab}]$ and $[k_{Ab}]$ and in equation (A2), involving the matrices $[c_{Bb}]$ and $[k_{Bb}]$.

(b) *LSR element*

Equation of motion:

$$[m_l]\{\ddot{d}_{Bl}\} + [c_l]\{\dot{d}_{Bl}\} + [k_l]\{d_{Bl}\} = \{f^t_{Bl}\}, \tag{A4}$$

where

$$\{f^t_{Bl}\} = \{f_{Bl}\} + \{f^c_{Bl}\} + \{f^k_{Bl}\}, \tag{A5}$$

and

$$\{f^c_{Bl}\} = \{f^c_{Al}\}, \qquad \{f^k_{Bl}\} = \{f^k_{Al}\}. \tag{A6}$$

(c) *RSR element*

Equation of motion:

$$[m_l]\{\ddot{d}_{Br}\} + [c_r]\{\dot{d}_{Br}\} + [k_r]\{d_{Br}\} = \{f^t_{Br}\}, \tag{A7}$$

where

$$\{f^t_{Br}\} = \{f_{Br}\} + \{f^c_{Br}\} + \{f^k_{Br}\}, \tag{A8}$$

and

$$\{f^c_{Br}\} = \{f^c_{Ar}\}, \qquad \{f^k_{Br}\} = \{f^k_{Ar}\}. \tag{A9}$$

The matrices and vectors involved in the above equations are all shown in Part B of the appendix.

The following is a summary of the mass and stiffness matrices of the twin-rail and bridge elements.

(a) *CFR element*

Track A:

$$\begin{aligned}
[m_A] &\equiv m_r[\psi^0_u] + m_r[\psi^0_v] + m_r[\psi^0_w] + I^*_r[\psi^0_\theta],\\
[k_A] &\equiv E_rA_r[\psi^1_u] + E_rI_{rz}[\psi^2_v] + E_rI_{ry}[\psi^2_w] + 2l_dk^*_{bh1}[\psi^0_u] + 2l_dk^*_{bv1}[\psi^0_v]\\
&\quad + 2l_dk^*_{bh1}[\psi^0_w] + \tfrac{2}{3}\, l^3_dk^*_{bv1}[\psi^0_\theta],\\
[c_A] &= [c_{A0}] + [c_{AA}] \equiv [c_{A0}] + 2l_dc^*_{bh1}[\psi^0_u] + 2l_dc^*_{bv1}[\psi^0_v] + 2l_dc^*_{bh1}[\psi^0_w] + \tfrac{2}{3}\, l^3_dc^*_{bv1}[\psi^0_\theta],
\end{aligned} \tag{A10}$$

where $[c_{A0}]$ accounts for the material damping and can be determined by the mass matrix $[m_A]$ and the stiffness matrix $[k_A]$, and

$$\begin{aligned}
[c_{Ab}] &\equiv 2l_dc^*_{bh1}[\psi^0_u] + 2l_dc^*_{bv1}[\psi^0_v] + 2l_dc^*_{bh1}[\psi^0_w] + \tfrac{2}{3}l^3_dc^*_{bv1}[\psi^0_\theta] - 2l_dl_bc^*_{bv1}[\psi^0_{v\theta}]\\
&\quad + 2hl_dc^*_{bh1}[\psi^0_{w\theta}],\\
[k_{Ab}] &\equiv 2l_dk^*_{bh1}[\psi^0_u] + 2l_dk^*_{bv1}[\psi^0_v] + 2l_dk^*_{bh1}[\psi^0_w] + \tfrac{2}{3}l^3_dk^*_{bv1}[\psi^0_\theta] - 2l_dl_bk^*_{bv1}[\psi^0_{v\theta}]\\
&\quad + 2hl_dk^*_{bh1}[\psi^0_{w\theta}].
\end{aligned} \tag{A11}$$

Track B:

$$[m_B] = [m_A], \quad [k_B] = [k_A], \quad [c_B] = [c_A] \tag{A12}$$

and

$$\begin{aligned}
[c_{Bb}] &\equiv 2l_dc^*_{bh1}[\psi^0_u] + 2l_dc^*_{bv1}[\psi^0_v] + 2l_dc^*_{bh1}[\psi^0_w] + \tfrac{2}{3}l^3_dc^*_{bv1}[\psi^0_\theta] + 2l_dl_bc^*_{bv1}[\psi^0_{v\theta}]\\
&\quad + 2hl_dc^*_{bh1}[\psi^0_{w\theta}],\\
[k_{Bb}] &\equiv 2l_dk^*_{bh1}[\psi^0_u] + 2l_dk^*_{bv1}[\psi^0_v] + 2l_dk^*_{bh1}[\psi^0_w] + \tfrac{2}{3}l^3_dk^*_{bv1}[\psi^0_\theta] - 2l_dl_bk^*_{bv1}[\psi^0_{v\theta}]\\
&\quad + 2hl_dk^*_{bh1}[\psi^0_{w\theta}].
\end{aligned} \tag{A13}$$

(b) *LSR element* (for Tracks A and B)

$$[m_l] \equiv m_r[\psi_u^0]_l + m_r[\psi_v^0]_l + m_r[\psi_w^0]_l + I_r^*[\psi_\theta^0]_l,$$

$$[k_l] \equiv E_r A_r[\psi_u^1]_l + E_r I_{rz}[\psi_v^2]_l + E_r I_{ry}[\psi_w^2]_l + 2l_d k_{bh1}^*[\psi_u^0]_l + 2l_d k_{bv1}^*[\psi_v^0]_l + 2l_d k_{bh1}^*[\psi_w^0]_l + \tfrac{2}{3} l_d^3 k_{bv1}^*[\psi_\theta^0]_l, \tag{A14}$$

$$[c_l] = [c_{l0}] + [c_{ll}] \equiv [c_{l0}] + 2l_d c_{bh1}^*[\psi_u^0]_l + 2l_d c_{bv1}^*[\psi_v^0]_l + 2l_d c_{bh1}^*[\psi_w^0]_l + \tfrac{2}{3} l_d^3 c_{bv1}^*[\psi_\theta^0]_l.$$

(c) *RSR element* (for Tracks A and B)

$$[m_r] \equiv m_r[\psi_u^0]_r + m_r[\psi_v^0]_r + m_r[\psi_w^0]_r + I_r^*[\psi_\theta^0]_r,$$

$$[k_r] \equiv E_r A_r[\psi_u^1]_r + E_r I_{rz}[\psi_v^2]_r + E_r I_{ry}[\psi_w^2]_r + 2l_d c_{bh1}^*[\psi_u^0]_r + 2l_d c_{bv1}^*[\psi_v^0]_r + 2l_d c_{bh1}^*[\psi_w^0]_r + \tfrac{2}{3} l_d^3 c_{bv1}^*[\psi_\theta^0]_r, \tag{A15}$$

$$[c_r] = [c_{r0}] + [c_{rr}] \equiv [c_{r0}] + 2l_d c_{bh1}^*[\psi_u^0]_r + 2l_d c_{bv1}^*[\psi_v^0]_r + 2l_d c_{bh1}^*[\psi_w^0]_r + \tfrac{2}{3} l_d^3 c_{bv1}^*[\psi_\theta^0]_r.$$

(d) *Bridge element*

$$[m_b] \equiv m_b[\psi_u^0] + m_b[\psi_v^0] + m_b[\psi_w^0] + I_b^*[\psi_\theta^0],$$

$$[k_b] \equiv E_b A_b[\psi_u^1] + E_b I_{bz}[\psi_v^2] + E_b I_{by}[\psi_w^2] + \frac{E_b I_{bx}}{2(1+v_b)}[\psi_\theta^1] + 4l_d k_{bh1}^*[\psi_u^0] + 4l_d k_{bv1}^*[\psi_v^0] + 4l_d k_{bh1}^*[\psi_w^0] + [(\tfrac{2}{3} l_d^3 + 2l_d l_b^2)\, k_{bv1}^* + 2h^2 l_d k_{bh1}^*][\psi_\theta^0], \tag{A16}$$

$$[c_b] = [c_{b0}] + [c_{bb}] \equiv [c_{b0}] + 4l_d k_{bh1}^*[\psi_u^0] + 4l_d k_{bv1}^*[\psi_v^0] + 4l_d k_{bh1}^*[\psi_w^0] + [(\tfrac{2}{3} l_d^3 + 2l_d l_b^2)\, k_{bv1}^* + 2h^2 l_d k_{bh1}^*][\psi_\theta^0].$$

and

$$[c_{bA}] = [c_{Ab}], \quad [k_{bA}] = [k_{Ab}], \quad [c_{bB}] = [c_{Bb}], \quad [k_{bB}] = [k_{Bb}], \tag{A17}$$

where subscript "b" indicates the "bridge", E_b the Young's modulus, A_b the sectional area, I_{bx}, I_{by} and I_{bz} the moment of inertia about the x-, y- and z-axis, m_b the per-unit-length mass (including the mass of the ballast), I_b^* the per-unit-length mass moment of inertia about the x-axis (including the contribution of the ballast), v_b the Poisson ratio. The matrix $[c_{A0}]$ represents the material damping of the bridge structure and is determined by the mass matrix $[m_b]$ and the stiffness matrix $[k_b]$. In the above equations (A10–A17), the matrices involved are given as follows:

$$[\psi_u^0] = \begin{matrix}(u_1 \\ \\ \end{matrix} \begin{matrix} u_2) \\ \\ \end{matrix} \begin{bmatrix} \frac{l}{3} & \frac{l}{6} \\ \frac{l}{6} & \frac{l}{3} \end{bmatrix}, \quad [\psi_u^1] = \begin{bmatrix} \frac{1}{l} & -\frac{1}{l} \\ -\frac{1}{l} & \frac{1}{l} \end{bmatrix}, \quad [\psi_\theta^0] = \begin{matrix}(\theta_1 \\ \\ \end{matrix} \begin{matrix} \theta_2) \\ \\ \end{matrix} \begin{bmatrix} \frac{l}{3} & \frac{l}{6} \\ \frac{l}{6} & \frac{l}{3} \end{bmatrix}, \quad [\psi_\theta^1] = \begin{bmatrix} \frac{1}{l} & -\frac{1}{l} \\ -\frac{1}{l} & \frac{1}{l} \end{bmatrix}, \tag{A18}$$

$$[\psi_v^0] = \frac{l}{420}\begin{matrix}(v_1 & \psi_1 & v_2 & \psi_2)\end{matrix}\begin{bmatrix} 156 & 22l & 54 & -13l \\ & 4l^2 & 13l & -3l^2 \\ & sym. & 156 & -22l \\ & & & 4l^2 \end{bmatrix}, \quad [\psi_w^2] = \begin{bmatrix} \frac{12}{l^3} & \frac{6}{l^2} & -\frac{12}{l^3} & \frac{6}{l^2} \\ & \frac{4}{l} & -\frac{6}{l} & \frac{2}{l} \\ & sym. & \frac{12}{l^3} & -\frac{6}{l^2} \\ & & & \frac{4}{l} \end{bmatrix}, \tag{A19}$$

$$[\psi_w^0] = \frac{l}{420}\begin{matrix}(w_1 & \varphi_1 & w_2 & \varphi_2)\end{matrix}\begin{bmatrix} 156 & -22l & 54 & 13l \\ & 4l^2 & -13l & -3l^2 \\ & sym. & 156 & 22l \\ & & & 4l^2 \end{bmatrix}, \quad [\psi_w^2] = \begin{bmatrix} \frac{12}{l^3} & \frac{6}{l^2} & -\frac{12}{l^3} & -\frac{6}{l^2} \\ & \frac{4}{l} & \frac{6}{l} & \frac{2}{l} \\ & sym. & \frac{12}{l^3} & \frac{6}{l^2} \\ & & & \frac{4}{l} \end{bmatrix}, \tag{A20}$$

$$[\psi_{v\theta}^2] = \begin{matrix}(v_1 & \psi_1 & v_2 & \psi_2)\times(\theta_1 & \theta_2)\end{matrix}\begin{bmatrix} \frac{7l}{20} & \frac{3l}{20} \\ \frac{l^2}{20} & \frac{l^2}{30} \\ \frac{3l}{20} & \frac{7l}{20} \\ -\frac{l^2}{30} & -\frac{l^2}{20} \end{bmatrix}, \qquad [\psi_{w\theta}^0] = \begin{matrix}(w_1 & \varphi_1 & w_2 & \varphi_2)\times(\theta_1 & \theta_2)\end{matrix}\begin{bmatrix} \frac{7l}{20} & \frac{3l}{20} \\ -\frac{l^2}{20} & -\frac{l^2}{30} \\ \frac{3l}{20} & \frac{7l}{20} \\ \frac{l^2}{30} & \frac{l^2}{20} \end{bmatrix}, \tag{A21}$$

$$[\psi_u^0]_l = \frac{1}{2\lambda_u}, \quad [\psi_u^1]_l = \frac{\lambda_u}{2}, \quad [\psi_\theta^0]_l = \frac{1}{2\lambda_\theta}, \tag{A22}$$

$$[\psi_v^0]_l = \begin{matrix}(v_2 & \psi_2)\end{matrix}\begin{bmatrix} \frac{3}{4\lambda_v} & -\frac{1}{4\lambda_v^2} \\ -\frac{1}{4\lambda_v^2} & \frac{1}{8\lambda_v^3} \end{bmatrix}, \quad [\psi_u^1]_l = \begin{bmatrix} \lambda_v^3 & -\lambda_v^2 \\ -\lambda_v^2 & \frac{3\lambda_v}{2} \end{bmatrix}, \quad [\psi_w^0]_l = \begin{matrix}(w_2 & \varphi_2)\end{matrix}\begin{bmatrix} \frac{3}{4\lambda_w} & \frac{1}{4\lambda_w^2} \\ \frac{1}{4\lambda_w^2} & \frac{1}{8\lambda_w^3} \end{bmatrix},$$

$$[\psi_w^2]_l = \begin{bmatrix} \lambda_w^3 & \lambda_w^2 \\ \lambda_w^2 & \frac{3\lambda_w}{2} \end{bmatrix}, \tag{A23}$$

$$(u_1) \qquad (\theta_1)$$

$$[\psi_u^0]_r = \frac{1}{2\lambda_u}, \quad [\psi_u^1]_r = \frac{\lambda_u}{2}, \quad [\psi_\theta^0]_r = \frac{1}{2\lambda_\theta}, \tag{A24}$$

$$(v_1 \quad \psi_1) \qquad\qquad (w_1 \quad \varphi_1)$$

$$[\psi_v^0]_r = \begin{bmatrix} \dfrac{3}{4\lambda_v} & \dfrac{1}{4\lambda_v^2} \\ \dfrac{1}{4\lambda_v^2} & \dfrac{1}{8\lambda_v^3} \end{bmatrix}, \quad [\psi_u^2]_r = \begin{bmatrix} \lambda_v^3 & \lambda_v^2 \\ \lambda_v^2 & \dfrac{3\lambda_v}{2} \end{bmatrix}, \quad [\psi_w^0]_r = \begin{bmatrix} \dfrac{3}{4\lambda_w} & -\dfrac{1}{4\lambda_w^2} \\ -\dfrac{1}{4\lambda_w^2} & \dfrac{1}{8\lambda_w^3} \end{bmatrix},$$

$$[\psi_w^2]_r = \begin{bmatrix} \lambda_w^3 & -\lambda_w^2 \\ -\lambda_w^2 & \dfrac{3\lambda_w}{2} \end{bmatrix}. \tag{A25}$$

The parenthesized symbols in the above expressions indicate the associated d.o.f.s of the twin-rail or bridge elements which have a total of 12 d.o.f.s: $\{d\} = \langle u_1 \ v_1 \ w_1 \ \theta_1 \ \varphi_1 \ \psi_1 \ u_2 \ v_2 \ w_2 \ \theta_2 \ \varphi_2 \ \psi_2 \rangle^{\mathrm{T}}$, and the characteristic numbers of the twin-beam foundation system are defined as

$$\lambda_u = \sqrt{\frac{2l_d k_{bh2}^*}{E_r A_r}}, \quad \lambda_v = \sqrt[4]{\frac{l_d k_{bh2}^*}{2E_r I_{rz}}}, \quad \lambda_w = \sqrt[4]{\frac{l_d k_{bh2}^*}{2E_r I_{ry}}}, \quad \lambda_\theta = \sqrt{\frac{2l_d^3 k_{bv2}^*}{3E_r I_{rz}}}. \tag{A26}$$